

1
2
3 **Rapid assessment of drivers and air quality effects of**
4 **regional daily changes in air pollutant emissions based on**
5 **near-real-time techniques: A case in Jiangsu Province, China**
6

7 Chen Gu¹, Yutong Wang^{1,5}, Yuan Ji¹, Lei Zhang^{1,2}, Shuanzhu Sun³, Yuandong Bian¹,
8 Zimeng Zhang¹, Jiewen Zhu³, Wenxin Zhao¹, Sheng Zhong⁴, Yu Zhao^{1,2*}
9

10 ¹ State Key Laboratory of Water Pollution Control and Green Resource Recycling and
11 School of Environment, Nanjing University, 163 Xianlin Rd., Nanjing, Jiangsu
12 210023, China

13 ² Collaborative Innovation Center of Atmospheric Environment and Equipment
14 Technology, CICAET, Nanjing, Jiangsu 210044, China

15 ³ Jiangsu Frontier Electric Power Technology Co., Ltd., 58 Suyuan Ave., Nanjing,
16 Jiangsu 211102, China

17 ⁴ Jiangsu Provincial Environmental Monitoring Center, 100 Zhonghe Rd., Nanjing
18 210013, China

19 ⁵ Key Laboratory of Formation and Prevention of Urban Air Pollution Complex,
20 Ministry of Ecology and Environment, Shanghai Academy of Environment Sciences,
21 Shanghai 200233, P. R. China
22

23 *Corresponding author: Yu Zhao

24 Phone: 86-25-89680650; Email: yuzhao@nju.edu.cn
25
26
27

28 **ABSTRACT**

29 Fast and timely estimation of changing air pollutant emissions is critical for
30 understanding the complex sources of air pollution and supporting air quality
31 improvement, while current regional emission inventory was commonly reported with
32 time lag or coarse temporal resolution. Here we developed a near-real-time approach
33 that calculates the daily emissions of anthropogenic air pollutants, and applied this
34 approach for Jiangsu province, a typical developed region in eastern China. We
35 estimated that the annual total anthropogenic emissions of SO₂, NO_x, primary fine
36 particles (PM_{2.5}), non-methane volatile organic compounds (NMVOCs), and NH₃
37 were 246, 727, 298, 1186, and 377 Gg, respectively, for Jiangsu in 2022. Compared to
38 the national emission inventory, application of the provincial-level daily emission
39 estimates provided better model performance of PM_{2.5} and ozone (O₃) simulation for
40 all the involved months. The NO_x, SO₂, PM_{2.5}, and NMVOCs emissions in Jiangsu
41 during April-May 2022 (the period of COVID-19 lockdown in Shanghai) were
42 respectively 8%, 6%, 6%, and 10% smaller than those in the same period of 2023.
43 Transportation and Industry respectively contributed 89% of NO_x emission reduction
44 and 93% NMVOCs reduction. Combining with machine learning algorithms,
45 moreover, we revealed that the changing agricultural NH₃ emissions dominated the
46 variability of daily PM_{2.5} concentration, and that off-road transportation contributed
47 substantially to variabilities of both PM_{2.5} and O₃ levels. The study proved advantages
48 of incorporation of near-real-time data and machine learning techniques on tracking
49 the fast-changing emissions and detecting the sources of varying air quality.

50 **1. Introduction**

51 Emissions of air pollutants from anthropogenic activity including traffic, industrial
52 plants, and residential and commercial fuel consumption are the main cause of
53 worsened air quality, especially in economically developed regions with dense
54 populations (Sokhi et al., 2022; Zheng et al., 2018). Emission inventory, which

55 contains complete information on magnitude, spatial pattern, and temporal change of
56 air pollutant emissions by sector, is essential for identifying the sources of air
57 pollution and effectiveness of emission controls on air quality through numerical
58 modeling (Zhao et al., 2013; Zhang et al., 2019). Traditionally, “bottom-up”
59 methodology (i.e., the emissions were calculated for the finest source categories and
60 then aggregated to bigger categories) provides robust time series of emission
61 estimates based on national statistics (An et al., 2021; Crippa et al., 2020; Kurokawa
62 et al., 2020). However, these emission estimates were usually reported with a time lag
63 of at least 3-5 years. The delay reflected the time needed to finalize accurate national
64 statistics (e.g., official energy consumption by fuel type) and that needed to collect
65 and process them for compiling emission inventories (Guevara et al., 2023). As a
66 result, in addition to the inherent uncertainties in emission inventories, this delay can
67 introduce extra uncertainty when these inventories are employed in air quality
68 modeling, as they may miss current emission characteristics (Tong et al., 2012). Such
69 limitation can be greatly exacerbated for periods with big and unexpected emission
70 fluctuations, resulting from temporary actions for major events or public health
71 incidents (Huang et al., 2021; Wang et al., 2025).

72 To better track the changing emissions for specific events or incidents (e.g.,
73 COVID-19 pandemic), researchers have developed alternative methods to obtain the
74 near-real-time emission estimates (Gaubert et al., 2021; Schneider et al., 2022). The
75 objective of these efforts is to understand the driving factors of the changing
76 emissions and their impact on air quality. Real-time activity information with high
77 temporal resolution started to be incorporated in the emission estimation, such as the
78 electricity load and generation data by national transmission system operators, the
79 real-time vehicle flows monitored from navigation applications, and the real-time ship
80 navigational information from automatic identification system (AIS) (Liu et al., 2020a;
81 Liu et al., 2020b; Zheng et al., 2021; Huang et al., 2021; Harkins et al., 2021; Guevara
82 et al., 2021). Although limited availability and huge capacity of these data hinder their
83 full use in emission inventory development, there is a big potential in expanding the

84 data source to improve the capability of capturing the fast-changing emissions.

85 Currently, studies have been conducted for carbon dioxides (CO₂) emissions and
86 near-real-time data platforms and products have been developed, particularly for
87 well-identified stationary sources such as fossil fuel combustion plants (BEIS, 2022;
88 CBS, 2024; CITEPA, 2024; Carbon Monitor, 2024). Comparatively, achieving
89 near-real-time estimates is more challenging for air pollutants due to the large
90 complexity and variability of their emission processes. A great variety of air pollutants
91 come from a wide range of sources, containing fuel combustion, industrial processes,
92 on-road and off-road traffic, solvent evaporation, and agricultural activities (Xu et al.,
93 2023; Zheng et al., 2020). The emissions can be greatly influenced by many factors
94 and change a lot. Those factors include the human behavior patterns, operating
95 conditions of plants, improved use of manufacturing and pollution control
96 technologies, and/or meteorological conditions (Liu et al., 2024; Lei et al., 2023;
97 Geng et al., 2024). Given the strong chemical reactivity and short atmospheric
98 lifetime of many air pollutants, there exist complicated relationships between
99 emissions and air quality, emphasizing the importance of tracking the fast-changing
100 emissions (Liu et al., 2020; Zhao et al., 2020a). Therefore, efforts are still in great
101 need to develop effective approach for estimating the near-real -time emissions.

102 For the past years, China has substantially enhanced emission control for industrial
103 (e.g., “ultra-low” emission retrofit for selected non-electrical industries) and
104 residential sources (e.g., promotion of advanced stoves and clean coals during heating
105 seasons). Those measures have clearly reduced emissions of many air pollutants,
106 resulting in a 17.2 µg/m³ decline of fine particle (PM_{2.5}) concentration between 2015
107 and 2020 over the country (Geng et al., 2024). In contrast, the emissions of NO_x and
108 PM_{2.5} from passenger transportation respectively grew by 178% and 152% from 2019
109 to 2022 (Zhang et al., 2023), and the maximum daily 8h mean ozone (MDA8 O₃)
110 concentrations increased 5.8% from 2021 to 2022 for the country (MEE, 2023). The
111 diverse changes in emissions and air quality highlight the necessity to quickly and
112 accurately reveal the drivers of changes in air pollutant emissions and their impact on

113 ambient air quality (Gu et al., 2023). This is particularly important for periods with
114 severe air pollution episodes and unexpected incidents that substantially changed
115 human activities like COVID-19 lockdown, as timely temporary actions to address
116 pollution might be urgently required.

117 Province serves as a crucial role in air quality management in China. Due to
118 difference in economic and energy structure and atmospheric conditions, local
119 governments often implement diverse strategies and actions to reduce regional air
120 pollution. This results in large variability in both emission and air quality changes
121 across different regions. (Liu et al., 2022; Wang et al., 2021). Studies relying on
122 national emission data offer limited guidance in developing emission control
123 measures and assessing their effectiveness in air quality improvement (An et al.,
124 2021). Jiangsu Province, located in the Yangtze River Delta (YRD) in eastern China,
125 is one of most economically developed regions across the country (Supplementary
126 Figure S1). It accounted for 10.2% of the gross domestic product (GDP) in mainland
127 China (ranking the second place in the country), and 8.1%, 12.4% and 11.6% of coal
128 consumption, cement and crude steel production in 2022, respectively (NBS, 2023).
129 Following the implementation of air pollution prevention measures, the $PM_{2.5}$
130 pollution in Jiangsu has significantly decreased since 2015. However, the
131 development of the petrochemical industry and transportation has led to rapid changes
132 in emissions, making Jiangsu as the province with the highest and fastest growing O_3
133 concentration in YRD in recent years (Zhou et al., 2017; Wang et al., 2022).

134 In this study, therefore, we selected Jiangsu as an example to demonstrate the
135 development of near-real-time emission inventory and its application on rapid
136 assessment of air quality. Based on our previous work that incorporated the best
137 available facility-level information to develop a comprehensive provincial emission
138 inventory (Gu et al., 2023), here we constructed an approach driven by real-time
139 activity data from multiple sources. In this study, “near-real-time” refers to two
140 fundamental aspects. First, the emissions were rapidly estimated based on dynamic
141 activity data, with a minimal delay. It greatly bridged the substantial temporal gap

142 between the occurrence of emissions and the release of official statistical data. Second,
143 it refers to high temporal resolution of the emission data. Unlike previous emission
144 inventories that commonly provided monthly or annual average estimates, the
145 near-real-time approach provided daily emission data and thereby captured the short
146 and temporary perturbations of emissions from anthropogenic activities. The
147 pollutants include SO₂, NO_x, primary PM_{2.5}, NH₃, and non-methane volatile organic
148 compounds (NMVOCs). We then applied the method to obtain the near-real-time
149 emission estimates for 2022-2023, and assessed the driving factors of the short-term
150 emission change during the COVID-19 lockdown period. Finally, we used an Extreme
151 Gradient Boosting (XGBoost) algorithm to explore the relationship between the
152 variability of daily PM_{2.5} and O₃ concentrations and their precursor emissions for
153 2022. The study provides insights for timely design and implementation of air
154 pollution control actions, and can be used for reference for other developed and
155 polluted regions in China and worldwide.

156 **2. Methodology and data**

157 **2.1 Framework of near-real-time emission estimation**

158 Figure 1 shows the methodological framework. In our previous study (Gu et al., 2023),
159 we collected, examined, and integrated most available information on emission
160 sources to enhance the completeness and reliability of the provincial emission
161 inventory. All the information, including raw material and energy consumption,
162 product output, and manufacturing and emission control technologies, played an
163 important role in the estimation of near real-time emissions. The specific methods by
164 sector are described in Section 2.2. To ensure the robustness of the near-real-time
165 activity data (e.g., traffic indices and CEMS records), a rigorous data quality control
166 protocol was implemented to handle missing values and outliers. Obvious anomalies,
167 defined as values exceeding three standard deviations from the 7-day moving average,
168 were screened and removed. For short-term data gaps (1-2 days), linear interpolation

169 was applied. For longer continuous missing periods (≥ 3 days), missing values were
170 gap-filled using the historical average of the same day-of-week in the adjacent weeks,
171 adjusted by the regional sector-specific variability.

172 Furthermore, we improved the spatial distribution of air pollutant emissions. Point
173 sources of power and industrial enterprises were allocated based on their latitudes and
174 longitudes. We further utilized Point of Interest (POI) data from Gaode Map
175 (<https://lbs.amap.com/>, last visited on October 2025) to obtain changes on
176 road/waterway networks, land use, and building footprints. The spatial information is
177 commonly updated every 2-3 months. The use of updated POI data greatly reduced
178 the error of spatial allocation of emissions that may result from the delayed
179 information from the constant spatial proxies (Wang et al., 2017).

180 **2.2 Near-real-time daily emission estimation by sector**

181 This section describes the methods for estimating near-real-time daily emissions for
182 2022 and 2023. Six major sectors were included (Power, Industrial plant, Vehicles
183 (On-road transportation), Off-road machinery, Residential, and Agriculture), covering
184 most anthropogenic activities. Road and construction site dusts were not contained.

185 **Power plant** Previously we developed a method of applying online measurement data
186 from the continuous emission monitoring systems (CEMS,
187 <http://218.94.78.61:8080/newPub/web/home.htm>, last visited on October 2025) for
188 emission estimation at the unit/plant level (Zhang et al., 2019). With this basis, we
189 have improved the emission estimation method to enable the stable and continuous
190 acquisition of near-real-time emission data lagged by one month. For the small
191 number of power-generating units without CEMS data, we assumed that their
192 pollutant concentrations in the flue gas were at the average level of units with similar
193 installed capacity (Tang et al., 2019). The emissions were calculated based on the
194 mean hourly flue gas concentration of air pollutant obtained from CEMS and the
195 theoretical flue gas volume of each unit/plant:

$$E_{i,j,day} = C_{i,j,month} \times AL_{j,month} \times V_{j,m}^0 \times P_{i,j,m,day} \quad (1)$$

$$AL_j = F_m / R_m \quad (2)$$

where E is the emission of air pollutant; i , j and m indicate the specific pollutant species, individual power plant or unit, and fuel type, respectively; C is the monthly average concentration in the flue gas; AL is the activity level (here monthly coal consumption); F is the monthly electricity generation for various fuels, as reported by NBS (2023); R is the fuel consumption rate for power generation, taken from Tong et al. (2021), V^0 is the theoretical volume of flue gas produced per unit of fuel consumption (Zhao et al., 2010); P is the temporal profile of emissions (the daily to monthly emission ratio), based on the hourly pollutant concentrations and volume of flue gas for the month and specific day.

Industrial plant With its gradually expanding penetration, CEMS has become able to support near-real-time emission estimation for industrial plants (Tang et al., 2022; Bo et al., 2021). Given its varying coverage across sectors, we have developed a method that can stably estimate the near-real-time emissions at the plant level with a lag of one month. This method classifies industrial plants into three categories based on their CEMS coverage, as described below.

(1) Industrial plants with CEMS information. The method is similar to power plants:

$$E_{i,j,day} = C_{i,j,month} \times AL_{j,month} \times V_{i,j,k}^0 \times P_{i,j,m,day} \quad (3)$$

where k denotes the industrial sector; AL is the activity level (here represents monthly product output) as reported by NBS (2023), and V^0 is the theoretical volume of flue gas produced per unit of product output, which can be found in the technical specifications for the application of emission permits (MEE, 2021).

(2) Industrial plants without CEMS while it was equipped at some plants within the same sector. Sector-level emission factors (emissions per unit of activity level, EF) were calculated using CEMS data from other plants. Monthly emissions were estimated based on the sector-level EF and monthly product output from official environmental statistics. The near-real-time daily emissions were then generated

224 according to the temporal profile of emissions (P) obtained from CEMS installed in
225 other available plants in the sector.

$$226 \quad E_{i,j,day} = AL_{j,month} \times EF_{i,k} \times P_{i,j,m,day} \quad (4)$$

$$227 \quad EF_{i,k} = E_{i,k,month} / AL_{k,month} \quad (5)$$

228 where $EF_{i,k}$ is the sector-average emission factor for plants with CEMS for sector k ,
229 $E_{i,k}$ and AL_k are the total emissions from industrial plants with CEMS and their
230 product output, respectively.

231 (3) Industrial sectors without CEMS data. Emissions were principally calculated
232 based on activity level and emission factor. The activity data were derived based on
233 monthly official statistics reported by NBS (2023). In addition, we analyzed the
234 historical emission source data to trace the evolution of manufacturing and emission
235 control technologies for various sectors, and the emission factors could be calculated
236 for near-real-time emission estimations:

$$237 \quad E_{i,day} = AL_{month} \times EF_{i,k} \times P_{i,m,day} \quad (6)$$

238 where EF represents the emission factor based on the technological evolution of the
239 plant, P is the temporal profile of emissions, based on the fraction of daily electricity
240 load out of the monthly total for specific sector.

241 **Vehicles (On-road transportation)** Daily vehicular emissions were estimated
242 utilizing the International Vehicle Emissions model (IVE) combined with the Gaode
243 live congestion index (Zhou et al., 2019; Kholod et al., 2016). The level of traffic
244 congestion was indicated by the additional time incurred during a trip under congested
245 conditions, expressed as a percentage relative to uncongested conditions (Huo et al.,
246 2022). The Gaode congestion index is available for over 350 cities in China, with a
247 temporal resolution of 5 minutes (<https://report.amap.com/index.do>, last visited on
248 October 2025). By integrating the congestion index with a Greenshield's traffic
249 density model (Yang et al., 2019), we estimated the traffic volume which serves as a
250 temporal allocation factor to calculate the daily emissions. This approach assumes that
251 vehicular activity data (e.g., mileage and fuel consumption) are accessible, albeit
252 typically with a lag in reporting, as such information is usually provided on an annual

253 basis. Consequently, the near-real-time emissions can be estimated based on the daily
254 variations of congested index and EFs compared to the previous year (Eq. 7):

$$255 \quad E_{i,m,day} = \frac{(I_{day, year-1}) \times I_{day,(year-1)}^2 \times EF_{i,m,day,year}}{(I_{day, (year-1)-1}) \times I_{day,year}^2 \times EF_{i,m,day,(year-1)}} \quad (7)$$

256 In Equation (7), EF represents the emission factor calculated by the IVE model. The
257 input parameters of IVE, such as vehicle population by type, registration dates, fuel
258 types, and emission standards, can be obtained from the transportation management
259 departments of individual cities. These historical data can be extrapolated to the
260 present date utilizing the vehicle survival curve, thereby bridging any gaps in the
261 current information (Sun et al., 2020). Because official high-frequency traffic activity
262 data are unavailable in near-real-time, we introduced I , the Gaode traffic congestion
263 index, as a dynamic activity scaling factor. This index reflects the comprehensive
264 traffic volume and operational status of the overall road network, allowing us to
265 dynamically scale the baseline emissions into daily-scale trajectories. The index
266 serves as a generalized proxy for total road network activity, and the same scaling
267 factor was applied uniformly for all vehicle types. Although different temporal
268 operational patterns might exist for various vehicle types (e.g., larger volume for
269 trucks during nighttime or on specific freight corridors), obtaining the near-real-time
270 activity information by vehicle type remains a challenge at the provincial level in
271 China. The baseline EF for vehicles in Equation 7 were derived using the IVE model,
272 which comprehensively accounts for the influences of complex driving conditions,
273 including vehicle speed and engine load. However, continuous recalculation of
274 real-time and speed-dependent EFs on a daily, province-wide scale is computationally
275 intensive and remains as a challenge. For the near-real-time estimation of traffic
276 emissions, therefore, the EFs were treated as baseline constants for 2022, and we
277 predominantly focused on the dynamic adjustment of activity levels and treated them
278 as the primary driving factor for the daily emission fluctuations.

279 **Off-road Transportation** Off-road transportation was divided into five categories:
280 construction machinery, agricultural machinery, marine, railway, and aviation.
281 Emissions from construction machinery were estimated based on assumed daily

282 utilization rates derived from the operating rates of construction sites (Shen et al.,
283 2023; Huang et al., 2021). The daily usage of agricultural machinery was assumed to
284 correlate with the application of nitrogen fertilizers from agricultural sources (see the
285 description of agriculture as below). Emissions from railway, marine and aviation
286 sources were estimated using data from passenger/cargo turnover, individual ports and
287 commercial flights, respectively. These data were obtained from the China
288 Entrepreneur Investment Club (CEIC) (<https://www.ceicdata.com.cn>, last visited on
289 October 2025), Marine Traffic (<http://www.marinetraffic.com>, last visited on October
290 2025) and Flightradar24 databases (<http://www.flightradar24.com>, last visited on
291 October 2025) (Huo et al., 2022; Liu et al., 2020a).

292 **Residential sources** We followed Shao et al. (2023) and developed a Bayesian
293 hierarchical model to estimate daily heating energy consumption by fuel type, based
294 on two primary factors influencing residential energy consumption: temperature and
295 GDP. The daily temperature data were taken from ERA5 products provided by the
296 European Centre for Medium-Range Weather Forecasts (ECMWF)
297 (<https://cds.climate.copernicus.eu>, last visited on October 2025), while GDP from the
298 national statistics published quarterly by the National Bureau of Statistics
299 (<http://www.stats.gov.cn/>, last visited on October 2025). For the months without GDP
300 data, we assumed a linear relationship between GDP and the nighttime light index (Xu
301 et al., 2024), and applied the National Polar-orbiting Partnership Visible Infrared
302 Imaging Radiometer Suite (NPP-VIIRS, <https://www.earthdata.nasa.gov/>, last visited
303 on October 2025) provided by National Aeronautics and Space Administration
304 (NASA) to extrapolate the GDP for those months. We applied the gridded population
305 dataset (1km×1km) released by a database of the Chinese Academy of Sciences
306 (<https://www.resdc.cn/Default.aspx>, last visited on October 2025) for 2020. To
307 account for the effect of large-scale population migration, we integrated the
308 Population Migration Index (PMI) developed by Baidu (<https://qianxi.baidu.com/#/>,
309 last visited on October 2025). This index calculates the proportion of incoming
310 migrants relative to the local population.

311 **Agriculture** NH₃ emissions from fertilizer use can be largely influenced by
312 meteorological conditions, soil environment, and farming practices. In our previous
313 study, we quantified NH₃ emissions using dynamic EFs associated with those factors
314 (Zhao et al., 2020b). In this study, we expanded the methodology and estimated NH₃
315 emissions by using daily EFs. Regarding the baseline activity data for NH₃
316 estimations, the information was systematically derived from official statistics. For
317 livestock and poultry breeding, we utilized the year-end stock. For synthetic fertilizers,
318 the application amount was calculated as the product of the city-level sown area of
319 cropland and the provincial application rate per unit area obtained from national
320 investigations. To convert these annual totals into dynamic near-real-time estimations,
321 we integrated the temporal allocation of activity data with real-time meteorological
322 conditions. Based on the regional farming database from the Ministry of Agriculture,
323 we tracked the specific growing seasons of major crop types to determine the exact
324 timing of basal dressing and top dressing. By combining the farming cycles with
325 meteorological conditions and high-resolution soil pH databases, we generated the
326 spatiotemporal pattern of NH₃ emissions.

327 **2.3 Air quality modeling**

328 To evaluate the near-real-time emission estimate, we used the Community Multiscale
329 Air Quality (CMAQ v5.1) model developed by US Environmental Protection Agency
330 (<https://www.epa.gov/cmaq>, last visited on October 2025), to simulate the PM_{2.5} and
331 O₃ concentrations in Jiangsu. Four months (January, April, July, and October) in 2022
332 were selected as the simulation periods, with a spin-up time of 7 days for each month
333 to reduce the impact of the initial condition on the simulation. As shown in
334 Supplementary Figure S1, three nested domains (D1, D2, and D3) were applied with
335 the horizontal resolutions at 27, 9, and 3 km, respectively, and the most inner D3
336 covered Jiangsu and parts of the YRD region including Shanghai, northern Zhejiang,
337 and eastern Anhui. The Multi-resolution emission inventory of China (MEIC, [http://
338 http://meicmodel.org.cn/](http://http://meicmodel.org.cn/), last visited on October 2025) was applied for D1, D2, and
339 the regions out of Jiangsu in D3 (Zheng et al., 2018), and the provincial-level

340 near-real-time emission estimate was applied for Jiangsu in D3. The Carbon Bond
341 Mechanism (CB05) and AERO5 mechanisms were used for the gas-phase chemistry
342 and aerosol module, respectively.

343 The meteorological field for the CMAQ was obtained from the Weather Research and
344 Forecasting model (WRF v3.4, <https://www.mmm.ucar.edu/models/wrf>, last visited on
345 October 2025). Meteorological initial and boundary conditions were obtained from
346 the National Centers for Environmental Prediction (NCEP,
347 <https://psl.noaa.gov/data/reanalysis/reanalysis.shtml>, last visited on October 2025)
348 datasets. Ground observations at 3-h intervals were downloaded from National
349 Climatic Data Center (NCDC, <ftp://ftp.ncdc.noaa.gov/pub/data/noaa/isd-lite/>, last
350 visited on October 2025). Statistical indicators including bias, index of agreement
351 (IOA), and root mean squared error (RMSE) were used to evaluate the WRF
352 performance (Gu et al., 2023). The discrepancies between simulations and ground
353 observations were within an acceptable range (Supplementary Table S1).

354 We collected ground observation data of hourly PM_{2.5} and O₃ concentrations at the
355 110 state-operating air quality monitoring stations within Jiangsu
356 (<https://data.epmap.org/page/index>, see the station locations in Figure S1, last visited
357 on October 2025). Correlation coefficients (R), normalized mean bias (NMB) and
358 normalized mean errors (NME) between observation and simulation for each month
359 were calculated to evaluate the performance of CMAQ modeling.

360 We further compared the modeling performance using the provincial-level
361 near-real-time emission estimates in D3 with that based on MEIC. Since MEIC was
362 currently available till 2020, direct application of MEIC introduce bias from the
363 discrepancy in annual total emissions for different years. To avoid this, we adjusted
364 the annual total emissions of various species in MEIC (for Jiangsu 2020) to perfectly
365 match those of our near-real-time estimates (for Jiangsu 2022), and kept the
366 spatiotemporal distribution of emissions unchanged (referred as “MEIC-revision”).
367 The treatment ensured that any improvement in modeling performance with the
368 near-real-time emission estimate resulted from its optimized spatiotemporal pattern of
369 emissions rather than the total levels.

370 **2.4 Removing meteorological influence on PM_{2.5} and O₃ concentrations**

371 To explore the influence of anthropogenic emission changes on the variability of
372 PM_{2.5} and O₃ levels in 2022, we removed the impact of varying meteorological
373 conditions by employing a stepwise multiple linear regression (MLR) model (Li et al.,
374 2021). The surface daily concentrations of O₃ and PM_{2.5} were taken from the Tracking
375 Air Pollution in China (TAP, <http://tapdata.org.cn/>, last visited on October 2025) with
376 a horizontal resolution of 1 km×1 km (Geng et al., 2021). We incorporated nine
377 meteorological variables from the ERA5 database at a resolution of 0.25°×0.25°,
378 considered as the potential covariates for O₃ and PM_{2.5}. They were 10-meter zonal and
379 meridional wind speeds, temperature, boundary layer height, sea level pressure, cloud
380 cover, precipitation, relative humidity, and dew point temperature. These variables
381 were then scaled to a 3km×3km grid system by bilinear interpolation. To prevent
382 overfitting, we conducted MLR with the three most influential meteorological
383 parameters to estimate the variability of daily PM_{2.5} and maximum daily 8-hour
384 average (MDA8) O₃ concentration for each grid cell. Anomaly (the difference
385 between the raw data and the moving average of 30 days around) of air pollutant
386 concentrations and meteorological factors were used in the model, to exclude the
387 effect of monthly variability. Residuals that cannot be explained by the meteorological
388 variables were assumed to be attributed to anthropogenic emission changes (Li et al.,
389 2020). The results could be interpreted as the sensitivity of air pollutant concentration
390 to the daily emission anomalies from the annual average value.

391 To evaluate the MLR performance, we collected daily PM_{2.5} and O₃ concentrations at
392 the above-mentioned 110 air quality monitoring stations in Jiangsu (Figure S1), and
393 the R and NMB between observation and MLR were calculated.

394 **2.5 Examining the response of MDA8 O₃ and PM_{2.5} concentration to changing** 395 **daily emissions**

396 **2.5.1 XGBoost model**

397 XGBoost model is an advanced and scalable machine learning framework based on
398 gradient-boosted decision trees, widely recognized for its efficiency in handling
399 structured data and modeling complex nonlinear relationships (Requia et al., 2020;
400 Wang et al., 2023). XGBoost excels at processing high-dimensional spatiotemporal
401 datasets, such as gridded emission inventories, by effectively capturing interactions
402 among heterogeneous emission sources and temporal dependencies. Moreover, the
403 inherent interpretability features facilitate seamless integration with explainable AI
404 tools (e.g., SHapley Additive exPlanations (SHAP) to quantify the marginal
405 contribution of each input feature to individual model predictions), enabling rigorous
406 attribution analysis of air pollutant concentration variability (Zhao et al., 2025). To
407 overcome the traditional “black box” limitation of tree-based machine learning
408 models, we utilized the SHAP algorithm to interpret the XGBoost outputs. Based on
409 the algorithm, we were able to explicitly attribute the day-to-day variations in ambient
410 pollutant concentrations to precursor emission changes from specific sectors, thereby
411 drawing physically meaningful and conclusions.

412 The SHAP value is calculated with following equation:

$$413 \quad y_i = y_{base} + f(X_{i,1}) + f(X_{i,2}) + \dots f(X_{i,n}) \quad (8)$$

414 where y_i is the predicted value of the model for the i th sample; $f(X_{i,n})$ is the
415 contribution of the n th eigenvalue in the i th sample to the final predicted value, with
416 positive or negative representing that the eigenvalue makes the predicted value
417 increase or decrease; and y_{base} is the baseline value of the predicted outputs for all
418 types of predictions, representing the average prediction results for each category
419 without the influence of any eigenvalue.

420 **2.5.2 Anthropogenic effects on PM_{2.5} and MDA8 O₃ variability**

421 The XGBoost-SHAP modeling framework was implemented at the horizontal
422 resolution of 3km×3km to capture the emission-concentration relationship. XGBoost

423 regression models were independently trained for each grid cell. January and July
424 were selected as typical months for ambient PM_{2.5} and O₃, respectively. Daily time
425 series of 20 pollutant-sector combinations (4 pollutant (SO₂, NO_x, NMVOCs, PM_{2.5})
426 × 5 sectors (Power, Industry, On-road (Vehicles), Off-road, Residential) except for
427 tiny On-road SO₂, and agricultural NH₃.) were set as predictors, and
428 anthropogenic-driven variability of PM_{2.5} or O₃ concentrations as target variables.
429 Similarly, the emission inputs were treated as anomaly (the difference between the
430 current day's emissions and the moving average of 30 days around). A 10-fold
431 cross-validation was applied (80% training and 20% testing), and the bias and
432 correlation coefficient (R) were calculated to evaluate the model performance (Xiao et
433 al., 2018).

434 SHAP values were calculated for each emission feature using the tree explainer
435 algorithm, quantifying contributions of pollutant-sector combinations to variability of
436 daily anthropogenic-driven concentrations. Note that SHAP values represented the
437 deviation of individual predictions from the baseline expectation. Positive values
438 indicated emission features that elevated pollutant concentrations above the baseline,
439 while negative values indicated features that reduced concentrations below the
440 baseline. Aggregation of daily SHAP values for various pollutant-sector combinations
441 produced the daily-level contribution of total anthropogenic emissions to the changing
442 ambient concentration, and the daily-level contributions could then be aggregated to
443 the monthly level.

444 **3. Results and discussions**

445 **3.1 Anthropogenic air pollutant emissions**

446 **3.1.1 Total air pollutant emissions in 2022**

447 The total anthropogenic emissions of SO₂, NO_x, PM_{2.5}, NMVOCs, and NH₃ in
448 Jiangsu for 2022 were estimated at 246, 727, 298, 1186, and 377 Gg (Supplementary
449 Figure S2), which were respectively reduced by 17%, 33%, 18%, 7%, and 11%

450 compared with those in 2019 (Gu et al., 2023). Note the emissions for multiple years
451 (2015, 2019, and 2022) were estimated with a consistent methodological framework
452 to make reasonable interannual comparison. Our estimates indicated that the reduction
453 rate of SO₂ emissions was much lower between 2019 and 2022 than that at 53%
454 between 2015 and 2019. In particular, the emissions from the power sector were
455 estimated to decline only 7% during 2019-2022. The result confirmed that the
456 abatement of SO₂ emissions have been clearly decelerated following the full
457 implementation of ultra-low emission retrofits, suggesting that the potential of further
458 reduction of SO₂ emissions for power sectors has become more limited. More energy
459 structure adjustment instead of end-of-pipe controls is needed for the sector.

460 In contrast to SO₂, the emissions of NO_x and PM_{2.5} were estimated to decline faster
461 during 2019-2022 than 2015-2019. Industrial sectors contributed largely to these
462 reductions, with the emission declining 27% and 22% for NO_x and PM_{2.5},
463 respectively (Figure S2). These reductions reflected expansion of intensified pollution
464 control policies from power to other sectors, particularly the ultra-low emission
465 standards implemented for steel (2019) and cement industries (2020)
466 (<https://sthjt.jiangsu.gov.cn/>, last visited on October 2025). By 2022, Jiangsu province
467 had implemented ultra-low emission retrofits in over 80% of iron & steel enterprises
468 and approximately 60% of cement clinker production lines (DEE, 2023). However,
469 slower progress of emission controls in coking, glass, and chemical industries
470 highlighted substantial emission reduction potential in these non-electrical industrial
471 sectors. Meanwhile, the NO_x emissions of transportation were estimated to decline by
472 41% from 2019 levels (53% for light-duty gasoline vehicles), driven mainly by the
473 nationwide implementation of China VI vehicle emission standard and increasing
474 penetration of renewable energy vehicles.

475 NMVOCs, as critical precursors of both secondary PM_{2.5} and O₃ formation, exhibited
476 a slower decline in emissions and have emerged as the priority of emission controls in
477 Jiangsu (Figure S2). Industrial activities dominate NMVOCs emissions in Jiangsu,
478 contributing 68% of the provincial total emissions. It resulted from the heavy

479 dependence of the province on chemical industries. For example, the province
480 accounted for over 40% of national pesticide active ingredient and dye production.
481 Notably, more than 60% of small-scale chemical enterprises persisted in utilizing
482 solvent-based coatings, inks, and adhesives with high-VOCs content (Simayi et al.,
483 2022; Hu et al., 2024). Furthermore, recent expansions in solvent consumption and
484 chemical output within large-scale enterprises along the Yangtze River have largely
485 offset the emission reductions through improvement of manufacturing and pollution
486 control technologies (Li et al., 2019). Consequently, intensified emission controls
487 should be urgently required for targeting key industrial sectors and critical regions for
488 NMVOCs reduction. Agricultural NH₃ emissions in Jiangsu have experienced a
489 decline of 14% during 2019-2022, primarily attributed to reduced nitrogen fertilizer
490 usage. However, the absence of effective NH₃ control measures prevented further
491 substantial reduction of emissions for the sector (Zhou et al., 2023; Zhao et al., 2022).

492 **3.1.2 Daily emission variability for air pollutants in 2022**

493 Figure 2 show the daily variability of total and sectoral emissions of various pollutants
494 (SO₂, NO_x, PM_{2.5}, NMVOCs, and NH₃) in 2022, respectively (the time series of
495 emissions (NO_x as an example) for all the involved source categories are provided in
496 Supplementary Figure S3). The results revealed distinct seasonal emission patterns of
497 air pollutants driven by anthropogenic activities and/or meteorological conditions.

498 The emissions of SO₂ and primary PM_{2.5} followed the seasonal patterns of fossil
499 energy consumption (Yun et al., 2021), with clear peaks in winter (from December to
500 February) associated with the substantial coal combustion for residential heating and
501 elevated industrial energy demand (Geng et al., 2021; Zhan et al., 2023). Regarding
502 NO_x, transportation has become the primary contributor to the emissions along with
503 improved emission controls from the power and industrial sectors. Following the
504 lifting of COVID-19 lockdown since June 2022, moreover, residents exhibited a
505 strong desire to travel, which enhanced the emissions from transportation. Compared
506 to the spring (from March to May), NO_x emissions from transportation increased 12%

507 during the summer (from June to August), consistent with the elevated population
508 mobility (Supplementary Figure S4). Additionally, the NO_x emission peak in March
509 reflected the resumption of industrial production and construction activities after the
510 Chinese New Year. The area of construction for residential and commercial buildings
511 increased 56% from February to March, with these activities heavily dependent on
512 diesel-powered machinery (Yang et al., 2015; Cliff et al., 2023). The NMVOCs
513 emissions were the largest in summer. Enhanced volatilization of solvents and
514 industrial chemicals by the warmer temperatures resulted in a 22% growth of summer
515 emissions compared to spring. Similar to NO_x, the NMVOCs emissions in March
516 rebounded with a 17% growth compared to February, reflecting the resumption of
517 coating, printing, and petrochemical industries. For NH₃, the highest emissions in
518 March and September were predominantly driven by the intensive spring sowing and
519 autumn farming seasons. In contrast, although the total fertilizer amount decreased in
520 summer (mainly limited to top dressing for specific crops like paddy rice), the high
521 temperature in summer together with top dressing greatly elevated the NH₃
522 volatilization rates, resulting in peak emission factors that kept the emissions at a high
523 level.

524 Notably, the province has made great efforts on reducing emissions during the period
525 with heavy pollution weather (DEE, 2022). The restriction measures included
526 alternating operations of energy-intensive industrial plants, such as cement, steel, and
527 glass production, in order to reduce the total production level and energy consumption
528 during the period. Furthermore, industrial parks were required to temporarily shut
529 down or to reduce the load of coal-fired boilers to mitigate regional precursor
530 emissions under the unfavorable meteorological conditions. Compared to August
531 2022, mandatory restrictions on coal-fired boilers and industrial plants for September
532 resulted in an 11% reduction of coal consumption for major industrial sectors, leading
533 to a decline of 7%, 10%, 15%, and 12% for anthropogenic emissions of SO₂, NO_x,
534 PM_{2.5}, and NMVOCs, respectively. This demonstrated the effectiveness of pollution
535 control measures conducted by the government on counteracting pollution episodes

536 around August and September, despite persistent meteorological challenges (Wang et
537 al., 2023). However, subsequent emission rebounds in winter for SO₂ (+24%
538 compared with those in Autumn) and PM_{2.5} emissions (+19%) underscored the
539 limitation of seasonal control strategies for combustion-derived pollutants,
540 emphasizing the imperative for clean energy promotion to achieve sustainable
541 emission abatement.

542 In April 2022, a great reduction in air pollutant emissions was estimated. Compared
543 with March, the emissions of SO₂, NO_x, PM_{2.5}, and NMVOCs decreased by 11%, 8%,
544 6%, and 12% respectively. This abrupt decline was temporally associated with the
545 COVID-19 induced lockdown implemented in Shanghai (March 28-June 1, 2022).
546 The lockdown substantially disrupted industrial production, transportation activities,
547 and daily routines in neighboring Jiangsu Province. The results showed that
548 short-term public health incidents exerted profound impact on air pollutant emissions
549 (Zhang et al., 2024; Ma et al., 2023).

550 **3.1.3 High-resolution maps of air pollutant emissions**

551 Based on the real-time geospatial information from the POI system (e.g., quarterly
552 updated road networks, land use types, and monthly revised construction sites), we
553 achieved the evolving spatial pattern of daily air pollutant emissions with a horizontal
554 resolution of 3 km×3 km. Figure 3 presents the spatial distribution of daily average
555 emissions of major sectors in Jiangsu Province for 2022. We selected NO_x as an
556 example to illustrate the sector heterogeneity. The NO_x emissions from power,
557 industrial, vehicle, off-road transportation and residential sources in Jiangsu were
558 calculated at 144, 109, 247, 183 and 45 Gg respectively. Aviation emissions (less than
559 1% of total NO_x) were excluded due to their tiny contribution to the total emissions.

560 The spatial pattern of emissions was closely associated with corresponding
561 anthropogenic activities. Agricultural machinery emissions were predominantly
562 located in northern agricultural zones and coastal areas, correlating with the
563 spatiotemporal distribution of farming activities. In contrast, emissions from other

564 sources were more concentrated in the southern cities, especially along the Yangtze
565 River with the most abundant power and industrial plants. The NO_x emissions from
566 five cities in southern Jiangsu (Nanjing, Suzhou, Wuxi, Changzhou, Zhenjiang)
567 accounted for 59% and 63% of provincial power and industrial emissions,
568 respectively. On-road transportation emissions demonstrated a strong dependence on
569 the road network. Nanjing and Xuzhou, as critical national railway transportation hubs,
570 contributed 24% and 13% of provincial NO_x emissions from railways (Wang et al.,
571 2016). In addition, Suzhou contributed 29% of provincial marine emissions, attributed
572 to its pivotal role in Yangtze River Delta inland waterway logistics (Shen et al., 2021).
573 Unsurprisingly, the residential NO_x emissions were closely correlated with the
574 population density.

575 **3.1.4 Assessment of monthly variability**

576 Figure 4 compares the monthly distributions of SO₂, NO_x, and PM_{2.5} emissions
577 estimated in this study with those in MEIC, as well as those of provincial averages of
578 ambient concentrations of corresponding species obtained from the state-operating
579 observation sites in Jiangsu. Due to the unavailability of MEIC for the year 2022, we
580 used the result for 2020 instead.

581 For SO₂ (Figure 4a) and PM_{2.5} (Figure 4e), similar monthly variation patterns were
582 found between emissions and observed concentrations in Jiangsu. The near-real-time
583 emission estimates effectively captured the short-term fluctuations in anthropogenic
584 activities, including the abrupt reduction in April associated with the COVID-19
585 lockdown and the seasonal change from the temporary pollution control measures in
586 autumn. While ambient concentrations were influenced by meteorology and
587 secondary formation as well, the relatively long atmospheric lifetimes of SO₂ and
588 PM_{2.5} (typically several days) allow them to reflect the impact of primary emission
589 variations. These results partly justified the capability of the approach to track the
590 effect of changing anthropogenic activities on air pollutant emissions. In contrast, the
591 highly reactive nature and shorter atmospheric lifetime of NO_x resulted in a

592 decoupling between its emissions and ambient concentrations. We found contrary
593 monthly distributions between NO_x emissions and the observed NO₂ concentrations
594 (Figure 4c). The largest emissions were estimated in summer months but the lowest
595 concentrations were observed for the same months across the year. This inconsistency
596 likely resulted from the following factors. Increased transportation activity in summer,
597 particularly mobility rebound after lockdown, elevated NO_x emissions. Meanwhile,
598 NO₂ was substantially consumed for O₃ formation through rapid photochemical
599 reactions under the intense solar radiation and high temperatures, and its atmospheric
600 lifetime was reduced to merely a few hours. In winter, there was more NO_x
601 accumulation in the atmosphere with weaker photochemical reactions and reduced
602 boundary layer heights (Ding et al., 2015; Wang et al., 2012).

603 Similar monthly distribution of emissions were found for the national (MEIC) and
604 provincial emission estimates (this work), implying regular patterns of monthly
605 anthropogenic activities could be captured by both inventories. Nevertheless,
606 disparities existed in the overall emission totals and sector distributions between the
607 two inventories. For instance, the contributions of industry to provincial emissions of
608 SO₂ and NO_x were estimated at 45% and 15% in this work, greatly different from the
609 MEIC estimation at 72% and 41%, respectively. These discrepancies might be
610 attributed to that the national inventory (MEIC) for 2020 has not yet fully included the
611 information of emission control technology upgrades (e.g., ultra-low emission
612 retrofits) in the industrial sector. Taking the sintering process in the steel industry as
613 an example, our facility-level estimations indicated that the average emission factors
614 for SO₂, NO_x, and PM_{2.5} were 0.143 kg/t, 0.228 kg/t, and 0.037 kg/t, respectively,
615 much lower than the recommended values of 1.34 kg/t, 0.55 kg/t, and 2.52 kg/t from
616 the guidelines for development of national emission inventory (He et al., 2018).

617 Substantial discrepancies were revealed for off-road transportation of SO₂ emissions.
618 The provincial SO₂ emission estimate from marine (12,877 Mg/yr) were almost three
619 times of that by MEIC (4,690 Mg/yr). As a major freight hub in the eastern coastal
620 region of the country, Jiangsu Province played a pivotal role in marine transportation,

621 and approximately 60% of vessels utilized heavy oil with high-sulfur content as fuel
622 (Dong et al., 2025). Application of national average EFs for the sector might lead to
623 underestimation in emissions. Furthermore, the national inventory ignored the
624 emissions from passing vessels at ports. Inclusion of such vessels would increase the
625 SO₂ emissions in the Yangtze River Delta region by a factor of 2.3 (Zhang et al.,
626 2017). As power and industrial sectors have gradually completed ultra-low emission
627 retrofits, marine emissions with less stringent controls may become more important in
628 the future, requiring greater efforts on fuel quality improvement and stricter emission
629 controls.

630 **3.2 Impacts of short-term lockdown on changes in emissions**

631 From March 28 to June 1 in 2022, Shanghai, the largest megacity in YRD and the
632 national center of economy, finance, manufacturing, and maritime trade in China,
633 implemented stringent COVID-19 lockdown measures that suspended intercity
634 mobility and industrial production and kept only essential logistics. This
635 unprecedented lockdown not only disrupted social and economic activities of
636 Shanghai, but also brought substantial effects for neighboring regions. Jiangsu
637 Province, a highly industrialized region adjacent to Shanghai, experienced severe
638 disruptions across service sectors, manufacturing supply chains, and maritime
639 logistics, resulting in substantial declines in energy consumption, industrial output,
640 and transportation activities. To further quantify the lockdown effect on air pollutant
641 emissions, we conducted a comparative analysis between two periods: the
642 lockdown-affected period (April-May 2022) and the post-pandemic period, the same
643 months one year later (April-May 2023).

644 The first column of Figure 5 (a1, b1, c1, d1) illustrates the variability in daily
645 emissions of NO_x, SO₂, PM_{2.5}, and NMVOCs in Jiangsu during April-May 2022
646 (lockdown period) versus 2023 (recovery period), as well as the difference between
647 the two periods. The emission differences (calculated as the relative change compared
648 to the 2023 level) reached 8%, 6%, 6%, and 10% for these air pollutants, respectively.

649 The most substantial decline in pollutant emissions occurred in April 2022, with a
650 gradually diminishing difference in May. However, the emissions by the end of May
651 2022 did not reach the level of recovery period in May 2023, reflecting the effect of
652 temporary measures on reducing economic activities even after the lifting of the
653 lockdown. The full economy recovery was delayed until 2023 when pandemic
654 restrictions were completely lifted (Li et al., 2023).

655 The second and third columns of Figure 5 (a2-d2 and a3-d3) illustrate the
656 contributions of various pollution source categories to the differences in emissions
657 between April-May of 2022 and 2023. Agricultural production remained basically
658 unaffected by the pandemic, thus the emission changes from agricultural machinery
659 were not included. The total reduction in NO_x emissions was 9,970 Mg,
660 predominantly attributed to transportation sources. The sector contributed to over 70%
661 of the emission reduction, including on-road transportation (15%), construction
662 machinery (27%), marine (19%), railway (5%), and aviation (4%). This result is
663 consistent with the findings on the effect of the 2020 COVID-19 lockdown (Lv et al.,
664 2020; Zhao et al., 2020a). However, there was a slight rebound in motor vehicle
665 emissions in May, which could be associated with basic everyday living and working
666 needs. Notably, construction machinery and marine were more affected by the
667 lockdown, attributable to construction material shortages (39% fewer of constructing
668 and building activities) and disrupted inland waterway logistics (20% less of port
669 throughput). Compared with transportation, the reduction of NO_x emissions from the
670 power (1,955 Mg) and the industrial sector (1,202 Mg) were smaller. The decline in
671 industrial electricity demand reduced the fossil fuel consumption and thereby the NO_x
672 emissions from the power sector. During industrial shutdowns and production
673 restrictions caused by the epidemic, frequent start-ups and shutdowns of production
674 and pollution control equipment resulted in a clear decline in NO_x removal efficiency
675 compared with normal operation condition of selective catalytic reduction (SCR)
676 systems. Previous measurements found that the average NO_x removal efficiency of
677 coal-fired units in iron & steel production enterprises decreased from 78% to 61%

678 (Shao et al., 2023), which to some extent offset the emission reduction effect of
679 industrial sources due to production restrictions.

680 SO₂ emission reductions predominantly originated from power (521 Mg, 21%) and
681 industrial sectors (1,710 Mg, 68%). For PM_{2.5}, transportation contributed 56% to the
682 total reduction of 3,583 Mg, with the contributions from on-road transportation,
683 construction machinery, marine, railway, and aviation accounting for 8%, 18%, 14%,
684 9%, and 7%, respectively. The emission reductions of NMVOCs were estimated at
685 20,170 Mg. The contribution of industrial sources reached 93%, largely due to a 64%
686 decline in crude oil processing in Jiangsu Province compared to 2023, as well as the
687 substantial declines in the production of chemical products (e.g., 27% less in
688 chemicals fibers and 65% less in ethylene manufacturing, NBS, 2023). The results
689 emphasized the lockdown impact on petrochemical industries reliant on cross-regional
690 material flows. In contrast, the emissions from residential sector were larger for the
691 lockdown period, with its coal consumption 7% more than that in recovery period one
692 year later, likely driven by the enhanced heating/cooking demands during mobility
693 restrictions.

694 In addition, an examination was conducted for exploring the diverse rebounds of
695 emissions for different sectors. Vehicle emissions exhibited a clear growth in May
696 compared to the central lockdown period in April. This early rebound in transportation
697 was likely driven by the gradual recovery of essential logistics and commuting. In
698 contrast, the emissions from industrial sector remained at a greatly suppressed level
699 throughout April and May, without an immediate rebound. This lag in industrial
700 recovery aligned with the socioeconomic condition of YRD, where the regional
701 industrial added value and GDP experienced a substantial decline in the second
702 quarter of 2022, followed by a slow recovery in the subsequent months (JSBS, 2022).
703 Such diversity between sectors indicated that mobile sources and energy supply could
704 respond quickly to the lifting of restrictions, while the recovery of large-scale
705 manufacturing could be more difficult due to complex supply chain realignment.

706 To further explore the spatial heterogeneity of the lockdown impacts, we conducted a

707 city-level comparative analysis by selecting three representative cities: Suzhou in
708 southern Jiangsu, Nantong in central Jiangsu, and Xuzhou in northern Jiangsu (see
709 locations of the cities in Figure S1). Suzhou is adjacent to Shanghai, with dense
710 petrochemical and manufacturing industries deeply embedded in regional supply
711 chains. Nantong is located in coastal area and relies heavily on marine logistics and
712 ports. Xuzhou is a city dominated by heavy industries and is farther from Shanghai
713 with less direct lockdown exposure compared to other cities in Jiaingsu.

714 As a core economic hub deeply integrated with Shanghai's supply chain, Suzhou was
715 greatly influenced by Shanghai lockdown (Table S2). The NMVOCs and NO_x
716 emissions in April-May 2022 dropped 17.9% (6,812 Mg) and 15.2% (2,917 Mg),
717 respectively, compared to the normal level (April-May 2023). This acute decline was
718 co-driven by the near-total freeze of cross-city highway freight, massive operational
719 bottlenecks at major ports, and widespread suspensions of petrochemical and
720 electronics manufacturing. Meanwhile, there existed notable drops in PM_{2.5} (-13.0%)
721 and SO₂ emissions (-9.0%) from halted construction and industrial fuel use. In
722 Nantong, the moderate declines in NO_x (-9.2%), NMVOCs (-8.6%), PM_{2.5} (-6.8%)
723 and SO₂ (-4.9%) primarily reflected disruptions in regional waterway logistics and
724 slowdowns in general manufacturing. In contrast, the emission reductions in Xuzhou
725 were much smaller around 3%, attributed to the continuous operations of heavy
726 industry to maintain the essential supply chains of industrial economy. These
727 diversities between cities demonstrated the capability of the research framework to
728 track the emission variation due to temporal and/or unexpected events at relatively
729 high spatiotemporal resolution.

730 In a summary, the results revealed complicated and diverse interventions of public
731 health incidents on energy use and activities for different sectors. The near-real-time
732 techniques developed in this work proved capable to capture the fast response of air
733 pollutant emissions to the short-term measures conducted during unexpected incidents,
734 and to clearly identify the driving sectors of emission changes compared to the normal
735 conditions.

736 **3.3 Evaluation of the near-real-time emission estimates with air** 737 **quality simulation**

738 The near-real-time estimates of provincial emissions were evaluated with air quality
739 simulation with CMAQ. To assess model performance, the observed concentrations of
740 hourly SO₂, NO₂, PM_{2.5}, and MDA8 O₃ were compared with the simulations based on
741 the provincial-level near-real-time emission estimates and MEIC for the selected four
742 months of 2022, as summarized in Supplementary Table S3. Overall, the simulation
743 with the provincial emission estimates shows acceptable agreement with the
744 observations, with the annual means of NMB and NME ranging -37.1% – 24.1% and
745 33.7% –53.5% for SO₂, -20.2% – 27.0% and 15.9% – 36.2% for NO₂, -18.6% –
746 10.8% and 37.5% –62.5% for PM_{2.5}, and -41.2% – -23.1% and 32.7% – 49.3% for O₃.
747 The analogous numbers for MEIC were -33.4% – 25.5% and 40.9% –51.8% for SO₂,
748 -19.9% – 35.6% and 22.3% – 55.1% for NO₂, -8.6% – 25.2% and 37.5% – 52.5% for
749 PM_{2.5}, and -39.9% – -28.1% and 44.3% – 54.5% for O₃, respectively. Most of the
750 NMB and NME were within the recommended criteria (-30%≤NMB≤30% and
751 NME≤50%, Emery et al., 2017). Better performance was achieved using the
752 provincial emission estimates developed in this work, implying the benefit of
753 applying the refined emission data on high-resolution air quality simulation.

754 Figures 6 and 7 compares the simulated daily PM_{2.5} and O₃ concentrations based on
755 the provincial (this work) and national emission estimates (MEIC) against
756 observations (results for SO₂ and NO₂ are shown in Supplementary Figures S5 and S6,
757 while spatial distributions for all the four pollutants are provided in Supplementary
758 Figures S7-S10). Compared to MEIC, the provincial-scale emission estimates
759 demonstrated better model performance in capturing the daily variability of pollutant
760 concentrations. The greater correlation coefficients (R) between simulated and
761 observed concentrations based on the near-real-time estimates indicated a remarkable
762 improvement for all the involved air pollutants (Table S3).

763 Figure 6 compares the observed and simulated PM_{2.5} concentrations, and measurable

764 improvement of model performance was achieved with the updated temporal profiles
765 for emissions. Specifically, the NMEs for January, April, July, and October decreased
766 from 37.5%, 55.3%, 62.5%, and 51.3% to 33.2%, 29.2%, 48.1%, and 42.6%,
767 respectively. The greatly improved model performance for April 2022 demonstrated
768 the capability of the near-real-time emission data to better capture the influence of
769 temporarily disrupted anthropogenic activities on air quality. During this period, the
770 COVID-19 lockdown in Shanghai severely restricted cross-regional freight transport
771 and industrial operations in Jiangsu (Huang et al., 2021). Compared with previous
772 emission inventories relying on historical temporal patterns, the refined daily emission
773 inventory with near-real-time techniques provided a more realistic representation of
774 the decline in primary aerosols and precursor emissions from heavy-duty vehicles and
775 point sources. Consequently, the simulated PM_{2.5} concentrations showed better
776 agreement with observations, with the NMB reduced to -6.6%. The refined emission
777 inventory also yielded notable corrections for periods with targeted administrative
778 interventions. During the late July period (July 20 to 31), for example, the NMB for
779 PM_{2.5} decreased from 47.3% with MEIC to 16.1% with the near-real-time emission
780 data, and the simulated mean concentrations dropped from 76.4 to 60.2 $\mu\text{g}/\text{m}^3$, much
781 closer to the observed 52.0 $\mu\text{g}/\text{m}^3$. This improvement was likely attributable to the
782 inventory's dynamic response to official electricity rationing policy. Driven by
783 extreme summer heat waves and power grid stress, local governments mandated load
784 reduction measures for energy-intensive facilities (Wei et al., 2020), causing an
785 irregular drop in industrial emissions that may not be tracked in previous inventories.
786 Similarly, the clear overestimation with MEIC for October was effectively mitigated.
787 The refined emission data appeared to better reflect the benefit of stringent control
788 measures implemented for preventing the heavy haze pollution in autumn and winter
789 (Jiang et al., 2023).

790 Figure 7 presents the observed and simulated O₃ concentrations. Compared with
791 MEIC, the NMEs with the near-real-time emission data for January, April, July, and
792 October decreased from 51.4%, 54.0%, 44.3%, and 54.5% to 49.3%, 41.1%, 32.7%,

793 and 34.6%, respectively. The updated emission data could have modulated the
794 simulation of non-linear photochemical processes. In January when weak solar
795 radiation generally limits photochemical O₃ production, NO_x titration often acts as a
796 dominating mechanism. The simulation with MEIC underestimated NO₂ by 37.4%,
797 and it potentially contributed to a 36.0% overestimation of O₃ due to insufficient
798 chemical scavenging. With the NO_x emissions 12% higher than MEIC during the
799 January, the near-real-time emission inventory resulted in a more reasonable
800 simulation of the titration effect. The enhanced chemical sink reduced the O₃ NMB to
801 -23.1% and improved the R² from 0.30 to 0.66. For April, the NO_x emissions were
802 15.9% lower in the real-near-time inventory than MEIC. Such a reduction in NO_x
803 could effectively weaken the titration inhibition, and it likely allowed the model to
804 better track the accelerated accumulation of O₃ driven by increasing spring solar
805 radiation. Simulation with the refined emission data yielded a growth of 1.72 μg/m³
806 for the month, much closer to the observation (2.59 μg/m³) than that with MEIC (0.33
807 μg/m³). Furthermore, there existed substantial correction of O₃ underestimation in
808 October, with the NME reduced from 54.5% to 34.6%. Such improvement resulted
809 potentially from the better simulated aerosol-radiation feedback. As mentioned earlier,
810 specific measures were conducted during autumn and winter in Jiangsu to prevent
811 heavy haze pollution. The emission abatement resulting from those measures were
812 captured by the near-real-time techniques, facilitating a lower aerosol loading in
813 CMAQ simulation compared to that with MEIC. This could theoretically elevate
814 photochemistry process and accelerate O₃ production, partially bridging the gap
815 between simulation and observation. In contrast, MEIC did not fully include the local
816 pollution control measures for specific seasons, and the relatively high aerosol loading
817 from simulation might have overly suppressed photochemical O₃ formation by
818 scattering and absorbing actinic flux (Zhao et al., 2021).

819 **3.4 Impact of daily emission change on the variability of PM_{2.5} and O₃** 820 **concentrations**

821 **3.4.1 Anthropogenic-driven contributions to variability of PM_{2.5} and MDA8 O₃** 822 **concentrations**

823 Figure 8 presents the contributions of the changing daily emissions to the monthly
824 variability of PM_{2.5} and MDA8 O₃ concentrations based on the MLR model. The
825 model performance was assessed with observed PM_{2.5} and O₃ concentrations
826 (Supplementary Figure S11). The simulated concentrations were strongly correlated
827 with observational data, with the correlation coefficient (R) of 0.79 for PM_{2.5} and 0.88
828 for MDA8 O₃. The validation indicated satisfying performance of MLR in capturing
829 provincial air quality variability.

830 The anthropogenic-driven variability of PM_{2.5} concentration was basically consistent
831 with the temporal variation of estimated emissions. As shown in Figure 8a, the
832 abundant emissions in January resulted in a prominent enhancement of 12.7 µg/m³ for
833 PM_{2.5} concentration, followed by December (1.8 µg/m³) and June (1.6 µg/m³). In
834 particular, the enhancement of June was driven largely by the post-pandemic
835 economic recovery, as discussed in in Section 3.2. For most warm months (April to
836 October, except June), negative impacts of anthropogenic activities on PM_{2.5} level
837 were found, ranging 1.1 – 4.2 µg/m³. Clear decline of PM_{2.5} due to emission change
838 was also found in February (5.5 µg/m³), resulting probably from the greatly reduced
839 human activities (industry and transportation) during the Chinese New Year holiday.
840 The PM_{2.5} growth occurred during winter heating period highlighted the necessity of
841 accelerating transition of clean household energy and improving management of
842 industrial production after the short-term lockdowns.

843 The variation of anthropogenic emissions was found to elevate O₃ concentrations in
844 most months of the year, particularly for warm seasons (Figure 8b). The
845 enhancements during March-August ranged 0.8 – 3.8 µg/m³, suggesting the important
846 role of human activities in aggravating O₃ pollution. High temperature in summer
847 promoted the emissions of temperature-dependent O₃ precursors, particularly
848 NMVOCs from various sources (Figure 2d). In addition, the NO_x emissions from
849 certain sources were elevated in warm seasons, e.g., those from off-road machinery in

850 the summer harvest season (Figure 2a). The growing abundance of precursors,
851 together with high temperature, enhanced the photochemical production rate of O₃.

852 However, the anthropogenic emissions during winter demonstrated a net negative
853 contribution to surface O₃ concentrations (e.g., -6.2 and -2.4 µg/m³ for November and
854 December, respectively), indicating a shift in the chemical regime of O₃ formation.
855 Although the NO_x emissions were not enhanced in winter (Figure 4), the weak
856 photochemical production under low temperature and solar radiation made the NO_x
857 titration more dominating in O₃ chemistry, primarily resulting in this net negative
858 contribution. Simultaneously, reduced NMVOCs emissions and diminished
859 photochemical activity restricted the efficiency of radical-driven O₃ production. The
860 resulting O₃-depleting reactions overwhelmed potential formation mechanisms,
861 leading to the estimated negative contribution from anthropogenic emissions. This
862 pattern contrasted sharply with the net positive effect of anthropogenic activities in
863 summer months, and underscored the complex season-dependent response of O₃ level
864 to the changing precursor emissions.

865 **3.4.2 Impact of fluctuations in anthropogenic emissions by precursor and sector** 866 **on PM_{2.5} and MDA8 O₃ concentrations**

867 The impacts of anthropogenic emission fluctuations on variability of PM_{2.5} and O₃
868 concentrations were quantified by precursor and sector, with a machine learning
869 framework integrating XGBoost and SHAP analysis. Derived from the 10-fold cross
870 validation, the correlation coefficient (R) between machine learning prediction and
871 observation reached 0.78 and 0.81 for daily PM_{2.5} and MDA8 O₃, respectively,
872 suggested satisfying capability of the machine learning framework in predicting the
873 anthropogenic-driven variability of PM_{2.5} and O₃ concentrations (Supplementary
874 Figure S12).

875 Figure 9a and 9b illustrates the contributions of changing emissions from different
876 pollutant-sector combinations to the variability of PM_{2.5} concentration in January and
877 that of MDA8 O₃ in July, respectively. The temporal variability of PM_{2.5} level

878 attributable to anthropogenic emission changes was in general consistent with that of
879 observed surface PM_{2.5} concentration (Figure 9a). For O₃, there existed some
880 discrepancy between the temporal distribution of anthropogenic-driven variability and
881 observed concentration in summer. This discrepancy may be attributed to the
882 substantial impacts of meteorological conditions and biogenic VOCs emissions on O₃
883 formation (Gu et al., 2023).

884 Among all the pollutant-sector combinations, fluctuations in agricultural NH₃
885 emissions accounted for 67.3% of the variability of PM_{2.5} concentrations in January,
886 followed by off-road NO_x (12.9%) and residential PM_{2.5} emissions (4.9%). The
887 contribution of NH₃ emission variation significantly exceeded those of NO_x (17.7%),
888 PM_{2.5} (10.8%), and SO₂ (4.2%), suggesting that Jiangsu may be transitioning to an
889 NH₃-rich regime following substantial reductions in SO₂ and NO_x emissions (Zhao et
890 al., 2020b). Therefore, agricultural NH₃ control has become the priority of the strategy
891 design for PM_{2.5} pollution alleviations, compared to traditional NO_x abatement. The
892 fluctuations in VOC-Industry contributed to 48.5% of the variability of MDA8 O₃
893 concentrations in July, followed by off-road VOCs (9.7%) and NO_x emissions (8.9%).
894 In total, the NMVOCs accounted for 69.7% of the anthropogenic-driven variability of
895 O₃ concentration, exceeding the contributions from NO_x (14.5%), PM_{2.5} (11.0%), and
896 SO₂ (4.9%). The positive contribution of NO_x to MDA8 O₃ indicated that the O₃
897 formation mechanism in Jiangsu may be shifting from a VOCs-limited regime
898 towards a transitional or NO_x-limited regime. Regarding the sector contributions with
899 various species aggregated, the agricultural emission fluctuations contributed most to
900 anthropogenic-driven variability of PM_{2.5} concentration (67.3%, Figure 9c), while
901 industrial activities contributed most to that of O₃ concentration (54.8%, Figure 9d).
902 Notably, off-road transportation emerged as an important contributor to both
903 pollutants (15.6% for PM_{2.5} and 24.4% for O₃), providing clear evidence for policy
904 making of coordinating control of PM_{2.5} and O₃ pollution.

905 **4. Conclusion remarks**

906 In this study, we incorporated near-real-time activity data from multiple sources and
907 developed a method for continuously estimating the regional daily air pollutant
908 emissions of anthropogenic origin. We then applied this method to estimate the
909 spatiotemporal evolution of emissions in Jiangsu Province, a typical developed area in
910 eastern China, with a particular focus on the period during the COVID-19 lockdown
911 in 2022 and the corresponding phase after the lifting of restrictions in 2023. Finally,
912 we constructed a rapid assessment approach that utilized machine learning algorithms
913 to quantify the impact of fast changing emissions on variability of daily air quality.

914 Our research indicated that emission controls have played a crucial role in abatement
915 of air pollutant emissions. The provincial emissions of SO₂, NO_x, PM_{2.5}, NMVOCs,
916 and NH₃ decreased 17%, 33%, 18%, 7%, and 11%, respectively, from 2019 to 2022.
917 Implementation of ultra-low emission retrofits for industrial sectors has proven
918 effective in reducing primary PM_{2.5} and NO_x emissions. However, there is an urgent
919 need to enhance NMVOCs emission control in key industrial sectors and areas. We
920 identified distinct temporal variabilities of emissions for various air pollutants. The
921 emissions of SO₂ and PM_{2.5} were influenced greatly by fossil fuel consumption
922 pattern, while NO_x emissions were increasingly dominated by that of transportation.
923 The NMVOCs emissions peaked in the summer and declined in winter, followed by a
924 rebound in emissions after the Chinese New Year. Our comparative analysis indicated
925 that the emissions of NO_x, SO₂, PM_{2.5}, and NMVOCs in Jiangsu during the
926 COVID-19 lockdown of Shanghai in April-May 2022 were respectively 8%, 6%, 6%,
927 and 10% smaller than those in the same months of 2023. Transportation was identified
928 as the primary contributors to the reductions in NO_x and PM_{2.5} emissions, while
929 industry accounted for 93% of the reduction in NMVOCs, closely associated with the
930 disrupted cross-regional product supply chains. Indicated by the contributions of
931 changing emissions from pollutant-sector combinations to the variability of PM_{2.5} and
932 O₃ levels, reducing agricultural NH₃ emissions should be critical for PM_{2.5} pollution
933 alleviation, and off-road transportation has become a priority target for coordinating

934 control of both PM_{2.5} and O₃ pollution.

935 The near-real-time techniques and estimation of daily-level emissions offer substantial
936 practical implications for current air quality management in China. Specifically, it can
937 be directly integrated into the “Emergency Response for Reducing Heavy Pollution
938 Weather” program. By providing the near-real-time feedback on emission variations,
939 policy makers can reasonably determine the short-term emission reduction measures
940 and timely evaluate their actual effectiveness (e.g., temporary suspension of specific
941 industries or traffic restrictions). Furthermore, combined with machine learning
942 techniques, this framework allows policy makers to decouple and distinguish the
943 environmental benefits of long-term policies of air quality improvement from
944 short-term emergency controls or unexpected socioeconomic shocks (like the
945 COVID-19 lockdown). The obtained knowledge provide a scientific basis for
946 formulating more cost-effective and precise coordinated control strategies for
947 reducing PM_{2.5} and O₃ pollution.

948 Furthermore, the framework could be potentially applied for predicting future
949 emissions under various hypothetical scenarios. Because the framework establishes a
950 dynamic linkage between sector-specific activity factors and emissions, it could
951 theoretically serve as a tool for predicting the emission change from policy
952 formulation. By adjusting these activity factors, such as the gradual penetration of
953 electric heavy-duty vehicles, the implementation of various industrial production
954 abatement during haze events, or targeted reductions in agricultural activities,
955 policy-makers could project the emission levels of diverse future scenarios. Coupled
956 with the rapid assessment approach with machine learning, the framework presents a
957 promising pathway to quantify how the simulated emission changes might affect the
958 daily variability of air quality, thereby better supporting the policy design and
959 adjustment for regional complex pollution controls.

960 The limitations of this work existed mainly in the near-real-time information of
961 multiple sources and the rapid assessment of air quality variability. For instance,
962 CEMS covered only relatively big point sources, thus we had to assume that the small
963 and fugitive sources followed similar variability of emissions with point sources. As

964 CEMS only covers SO₂, PM_{2.5}, and NO_x, the use of electricity consumption data for
965 NMVOCs may introduce substantial uncertainty. Future improvement in online
966 monitoring of NMVOCs will enhance the estimation of temporal variation of
967 emissions. While our research framework demonstrates robust performance in
968 data-rich regions like Jiangsu Province, its heavy reliance on extensive CEMS
969 coverage and provincial traffic monitors poses a limitation for its transferability to
970 less developed regions or other developing countries without sufficient data support.
971 To adapt this methodology for those regions, future applications could be expanded to
972 other datasets with global accessibility. For instance, satellite-derived tropospheric
973 NO₂ columns, daily nighttime light fluctuations, and generalized mobile phone
974 signaling data could serve as alternative proxies to estimate the activity levels and
975 their temporal profiles. Expanding this framework to incorporate such multi-source
976 remote sensing data will be more crucial for establishing near-real-time emission
977 inventories in regions with less data support. Moreover, the machine learning process
978 ignored the contributions from regional transport, which could result in some bias in
979 analyzing the impacts of anthropogenic emissions on air quality. However, in contrast
980 to time-consuming numerical modeling, machine learning offered a rapid and reliable
981 assessment of the impact of daily emission changes on air quality, which exactly
982 addressed the requirement of air quality management, and was recommended in future
983 policy making of air pollution controls.

984 **Data availability**

985 The gridded emission data for Jiangsu Province 2022-2023 can be downloaded at
986 <http://www.airqualitynju.com>

987 **Author contributions**

988 CGu developed the methodology, conducted the research and wrote the draft. YZhao
989 and LZhang developed the strategy and designed the research, and YZhao revised the
990 manuscript. YWang provided the support of machine learning modeling. YJi provided

991 the support of WFR-CMAQ. ZZhang, and WZhao supported emission data processing.
992 SSun, YBian, JZhu, and SZhong provided the support of emission data.

993 **Competing interests**

994 The authors declare that they have no conflict of interest.

995 **Acknowledgments**

996 This work was sponsored by the National Natural Science Foundation of China (grant
997 no. 42577116), the National Key Research and Development Program of China
998 (2023YFC3709802), the Key Research and Development Programme of Jiangsu
999 Province (BE2022838), and the Key Laboratory of Formation and Prevention of
1000 Urban Air Pollution Complex, Ministry of Ecology and Environment (no.
1001 2025080167).

1002 **References**

- 1003 An, J., Huang, Y., Huang, C., Wang, X., Yan, R., Wang, Q., Wang, H., Jing, S., Zhang,
1004 Y., Liu, Y., Chen, Y., Xu, C., Qiao, L., Zhou, M., Zhu, S., Hu, Q., Lu, J., and
1005 Chen, C.: Emission inventory of air pollutants and chemical speciation for
1006 specific anthropogenic sources based on local measurements in the Yangtze
1007 River Delta region, China, *Atmos. Chem. Phys.*, 21, 2003–2025,
1008 <https://doi.org/10.5194/acp-21-2003-2021>, 2021.
- 1009 BEIS: Provisional UK greenhouse gas emissions national statistics,
1010 <https://www.gov.uk/government/statistics/> (last visited on October 2025), 2022.
- 1011 Bo, X., Jia, M., Xue, X., Tang, L., Mi, Z., Wang, S., Cui, W., Chang, X., Ruan, J.,
1012 Dong, G., Zhou, B., and Davis, S.: Effect of strengthened standards on Chinese
1013 ironmaking and steelmaking emissions, *Nat. Sustain.*, 4, 811–820,
1014 <https://doi.org/10.1038/s41893-021-00736-0>, 2021.
- 1015 Carbon monitor: Global high spatial resolution near real time carbon map,

1016 <https://www.carbonmonitor.org.cn/> (last visited on October 2025), 2024.

1017 CBS: Emissions of greenhouse gases according to IPCC guidelines, quarter,
1018 <https://www.cbs.nl/nl-nl/cijfers/detail/> (last visited on October 2025), 2024.

1019 Chu, B., Ma, Q., Liu, J., Ma, J., Zhang, P., Chen, T., Feng, Q., Wang, C., Yang, N., Ma,
1020 H., Ma, J., Russell, A. G., and He, H.: Air Pollutant Correlations in China:
1021 Secondary Air Pollutant Responses to NO_x and SO₂ Control, *Environ. Sci.*
1022 *Technol. Lett.*, 7, 695-700, <https://doi.org/10.1021/acs.estlett.0c00403>, 2020.

1023 CITEPA: Monthly emissions barometer, <https://www.citepa.org/fr/barometre/> (last
1024 access: October 2025), 2024.

1025 Cliff, S. J., Drysdale, W., Lee, J. D., Helfter, C., Nemitz, E., Metzger, S., and Barlow,
1026 J. F.: Pandemic restrictions in 2020 highlight the significance of non-road NO_x
1027 sources in central London, *Atmos. Chem. Phys.*, 23, 2315–2330,
1028 <https://doi.org/10.5194/acp-23-2315-2023>, 2023.

1029 Crippa, M., Solazzo, E., Huang G., Guizzardi D., Koffi E., Muntean M., Schieberle C.,
1030 Friedrich R.: High resolution temporal profiles in the Emissions Database for
1031 Global Atmospheric Research, *Sci. Data*, 7, 121,
1032 <https://doi.org/10.1038/s41597-020-0462-2>, 2020.

1033 Department of Ecology and Environment of Jiangsu province (DEE): Report on the
1034 State of the Ecology and Environment in Jiangsu province, 2023.

1035 Department of Ecology and Environment of Jiangsu province (DEE): Emergency
1036 Plan for Severe Air Pollution in Jiangsu Province, 2022.

1037 Department of Industry and Information Technology of Jiangsu province (DII):
1038 Notice on Enterprises and Vehicles Intending to Apply for the 2022 Central
1039 Government Subsidy Settlement Fund for the Promotion and Application of New
1040 Energy Vehicles, 2023.

1041 Ding, J., van der A, R. J., Mijling, B., Levelt, P. F., and Hao, N.: NO_x emission
1042 estimates during the 2014 Youth Olympic Games in Nanjing, *Atmos. Chem.*
1043 *Phys.*, 15, 9399–9412, <https://doi.org/10.5194/acp-15-9399-2015>, 2015.

1044 Dong, X., Zhang, Y., Yu, G., Xiong, Y., Han, Z., Huo, J., Huang, C., Kan, H., Zheng,
1045 M., Ning, Z., and Xie, B.: Environmental and health impacts of reduced PM_{2.5}

1046 and trace metals from ship emissions under low-sulfur fuel oil policy in Shanghai,
1047 China, *Environmental Pollution*, 377, 126409,
1048 <https://doi.org/10.1016/j.envpol.2025.126409>, 2025.

1049 Dou, X., Wang, Y., Ciais, P., Chevallier, F., Davis, S. J., Crippa, M.,
1050 Janssens-Maenhout, G., Guizzardi, D., Solazzo, E., Yan, F., Huo, D., Zheng, B.,
1051 Zhu, B., Cui, D., Ke, P., Sun, T., Wang, H., Zhang, Q., Gentine, P., Deng, Z., and
1052 Liu, Z.: Near-real-time global gridded daily CO₂ emissions, *The Innovation*, 3,
1053 100182, <https://doi.org/10.1016/j.xinn.2021.100182>, 2022.

1054 Emery, C., Liu, Z., Russell, A. G., Odman, M. T., Yarwood, G., and Kumar, N.:
1055 Recommendations on statistics and benchmarks to assess photochemical model
1056 performance, *J. Air Waste Manag. Assoc.*, 67, 582-598,
1057 <https://doi.org/10.1080/10962247.2016.1265027>, 2017.

1058 Gaubert, B., Bouarar, I., Doumbia, T., Liu, Y., Stavrakou, T., Deroubaix, A., Darras, S.,
1059 Elguindi, N., Granier, C., Lacey, F., Müller, J. F., Shi, X., Tilmes, S., Wang, T.,
1060 and Brasseur, G. P.: Global changes in secondary atmospheric pollutants during
1061 the 2020 COVID-19 pandemic, *J. Geophys. Res. Atmos.*, 126, e2020JD034213.
1062 <https://doi.org/10.1029/2020JD034213>, 2021.

1063 Geng, G., Xiao, Q., Liu, S., Liu, X., Cheng, J., Zheng, Y., Xue, T., Tong, D., Zheng, B.,
1064 Peng, Y., Huang, X., He, K., and Zhang, Q.: Tracking Air Pollution in China:
1065 Near Real-Time PM_{2.5} Retrievals from Multisource Data Fusion, *Environ. Sci.*
1066 *Technol.*, 55, 12106-12115, <https://doi.org/10.48550/arXiv.2103.06520>, 2021.

1067 Geng, G., Liu, Y., Liu, Y., Liu, S., Cheng, J., Yan, L., Wu, N., Hu, H., Tong, D., Zheng,
1068 B., Yin, Z., He, K., and Zhang, Q.: Efficacy of China's clean air actions to tackle
1069 PM_{2.5} pollution between 2013 and 2020, *Nature Geoscience*, 17, 987–994,
1070 <https://doi.org/10.1038/s41561-024-01540-z>, 2024.

1071 Gu, C., Zhang, L., Xu, Z., Xia, S., Wang, Y., Li, L., Wang, Z., Zhao, Q., Wang, H., and
1072 Zhao, Y.: High-resolution regional emission inventory contributes to the
1073 evaluation of policy effectiveness: a case study in Jiangsu Province, China,
1074 *Atmos. Chem. Phys.*, 23, 4247–4269, <https://doi.org/10.5194/acp-23-4247-2023>,
1075 2023.

1076 Guevara, M., Jorba, O., Soret, A., Petetin, H., Bowdalo, D., Serradell, K., Tena, C.,
1077 Denier van der Gon, H., Kuenen, J., Peuch, V.-H., and Pérez García-Pando, C.:
1078 Time-resolved emission reductions for atmospheric chemistry modelling in
1079 Europe during the COVID-19 lockdowns, *Atmos. Chem. Phys.*, 21, 773–797,
1080 <https://doi.org/10.5194/acp-21-773-2021>, 2021.

1081 Guevara, M., Petetin, H., Jorba, O., Denier van der Gon, H., Kuenen, J., Super, I.,
1082 Granier, C., Doumbia, T., Ciais, P., Liu, Z., Lamboll, R. D., Schindlbacher, S.,
1083 Matthews, B., and Pérez García-Pando, C.: Towards near-real-time air pollutant
1084 and greenhouse gas emissions: lessons learned from multiple estimates during
1085 the COVID-19 pandemic, *Atmos. Chem. Phys.*, 23, 8081–8101,
1086 <https://doi.org/10.5194/acp-23-8081-2023>, 2023.

1087 Harkins, C., McDonald, B. C., Henze, D. K., and Wiedinmyer, C.: A fuel-based
1088 method for updating mobile source emissions during the COVID-19 pandemic,
1089 *Environ. Res. Lett.*, 16, 065018, <https://doi.org/10.1088/1748-9326/ac0660>,
1090 2021.

1091 He K., Zhang Q., Wang S.: Technical manual for the preparation of urban air pollution
1092 Source emission inventory, China Statistics Press, Beijing, 2018 (in Chinese).

1093 Hu, W., Zhao, Y., Lu, N., Wang, X., Zheng, B., Henze, D. K., Zhang, L., Fu, T.-M.,
1094 and Zhai, S.: Changing Responses of PM_{2.5} and Ozone to Source Emissions in
1095 the Yangtze River Delta Using the Adjoint Model, *Environ. Sci. Technol.*, 58,
1096 628-638, <https://doi.org/10.1021/acs.est.3c05049>, 2024.

1097 Huang, C., An, J., Wang, H., Liu, Q., Tian, J., Wang, Q., Hu, Q., Yan, R., Shen, Y.,
1098 Duan, Y., Fu, Q., Shen, J., Ye, H., Wang, M., Wei, C., Cheng, Y., and Su, H.:
1099 Highly Resolved Dynamic Emissions of Air Pollutants and Greenhouse Gas CO₂
1100 during COVID-19 Pandemic in East China, *Environ.Sci.Technol.Lett.*, 8,
1101 853-860, <https://doi.org/10.1021/acs.estlett.1c00600>, 2021.

1102 Huo, D., Huang, X., Dou, X., Ciais, P., Li, Y., Deng, Z., Wang, Y., Cui, D., Benkhelifa,
1103 F., Sun, T., Zhu, B., Roest, G., Gurney, K. R., Ke, P., Guo, R., Lu, C., Lin, X.,
1104 Lovell, A., Appleby, K., DeCola, P. L., Davis, S. J., and Liu, Z.: Carbon Monitor
1105 Cities near-real-time daily estimates of CO₂ emissions from 1500 cities

1106 worldwide, *Sci. Data*, 9, 533, <https://doi.org/10.1038/s41597-022-01657-z>, 2022.

1107 Jiang, S., Kong, S., Zheng, H., Wu, J., Yao, L., Chen, N., Zhu, B., Zhao, T., Bai, Y.,
1108 Liu, D., and Qi, S.: Winter-autumn air pollution control plan in North China
1109 modified the PM_{2.5} compositions and sources in Central China, *Atmos. Environ.*,
1110 306, 119827, <https://doi.org/10.1016/j.atmosenv.2023.119827>, 2023.

1111 Kholod, N., Evans, M., Gusev, E., Yu, S., Malyshev, V., and Barinov, A.: A
1112 methodology for calculating transport emissions in cities with limited traffic data:
1113 Case study of diesel particulates and black carbon emissions in Murmansk, *Sci.*
1114 *Total Environ.*, 547, 305-313, <https://doi.org/10.1016/j.scitotenv.2015.12.151>,
1115 2016.

1116 Kurokawa, J. and Ohara, T.: Long-term historical trends in air pollutant emissions in
1117 Asia: Regional Emission inventory in ASia (REAS) version 3, *Atmos. Chem.*
1118 *Phys.*, 20, 12761–12793, <https://doi.org/10.5194/acp-20-12761-2020>, 2020.

1119 Lei, T., Wang, D., Yu, X., Ma, S., Zhao, W., Cui, C., Meng, J., Tao, S., and Guan, D.:
1120 Global iron and steel plant CO₂ emissions and carbon-neutrality pathways,
1121 *Nature*, 622, 514–520, <https://doi.org/10.1038/s41586-023-06486-7>, 2023.

1122 Li, K., Jacob, D. J., Shen, L., Lu, X., De Smedt, I., and Liao, H.: Increases in surface
1123 ozone pollution in China from 2013 to 2019: anthropogenic and meteorological
1124 influences, *Atmos. Chem. Phys.*, 20, 11423–11433,
1125 <https://doi.org/10.5194/acp-20-11423-2020>, 2020.

1126 Li, K., Jacob, D. J., Liao, H., Qiu, Y., Shen, L., Zhai, S., Bates, K. H., Sulprizio, M. P.,
1127 Song, S., Lu, X., Zhang, Q., Zheng, B., Zhang, Y., Zhang, J., Lee, H. C., and Kuk,
1128 S. K.: Ozone pollution in the North China Plain spreading into the late-winter
1129 haze season, *Proc. Natl. Acad. Sci.*, 118, e2015797118,
1130 <https://doi.org/10.1073/pnas.2015797118>, 2021.

1131 Li, M., Zhang, Q., Zheng, B., Tong, D., Lei, Y., Liu, F., Hong, C., Kang, S., Yan, L.,
1132 Zhang, Y., Bo, Y., Su, H., Cheng, Y., and He, K.: Persistent growth of
1133 anthropogenic non-methane volatile organic compound (NMVOC) emissions in
1134 China during 1990–2017: drivers, speciation and ozone formation potential,
1135 *Atmos. Chem. Phys.*, 19, 8897–8913, <https://doi.org/10.5194/acp-19-8897-2019>,

1136 2019.

1137 Li, H. and Zheng, B.: TROPOMI NO₂ Shows a Fast Recovery of China's Economy in
1138 the First Quarter of 2023, *Environ. Sci. Technol. Lett.*, 10, 635-641,
1139 <https://doi.org/10.1021/acs.estlett.3c00386>, 2023.

1140 Liu, F., Page, A., Strode, S. A., Yoshida, Y., Choi, S., Zheng, B., Lamsal, L. N., Li, C.,
1141 Krotkov, N. A., Eskes, H., van der A, R., Veefkind, P., Levelt, P. F., Hauser, O. P.,
1142 and Joiner, J.: Abrupt decline in tropospheric nitrogen dioxide over China after
1143 the outbreak of COVID-19, *Sci. Adv.*, 6, eabc2992,
1144 <https://doi.org/10.1126/sciadv.abc2992>, 2020.

1145 Liu, M., Shang, F., Lu, X., Huang, X., Song, Y., Liu, B., Zhang, Q., Liu, X., Cao, J.,
1146 Xu, T., Wang, T., Xu, Z., Xu, W., Liao, W., Kang, L., Cai, X., Zhang, H., Dai, Y.,
1147 and Zhu, T.: Unexpected response of nitrogen deposition to nitrogen oxide
1148 controls and implications for land carbon sink, *Nat. Commun.*, 13, 3126,
1149 <https://doi.org/10.1038/s41467-022-30854-y>, 2022.

1150 Liu, X., Yang, L., Du, J., Zhang, H., Hu, J., Chen, A., and Lv, W.: Carbon and air
1151 pollutant emissions forecast of China's cement industry from 2021 to 2035,
1152 *Resources, Conservation and Recycling*, 204, 107498,
1153 <https://doi.org/10.1016/j.resconrec.2024.107498>, 2024.

1154 Liu, Z., Ciais, P., Deng, Z., Davis, S. J., Zheng, B., Wang, Y., Cui, D., Zhu, B., Dou,
1155 X., Ke, P., Sun, T., Guo, R., Zhong, H., Boucher, O., Bréon, F.-M., Lu, C., Guo,
1156 R., Xue, J., Boucher, E., Tanaka, K., and Chevallier, F.: Carbon Monitor, a
1157 near-real-time daily dataset of global CO₂ emission from fossil fuel and cement
1158 production, *Sci. Data*, 7, 392, <https://doi.org/10.1038/s41597-020-00708-7>,
1159 2020a.

1160 Liu, Z., Ciais, P., Deng, Z., Lei, R., Davis, S. J., Feng, S., Zheng, B., Cui, D., Dou, X.,
1161 Zhu, B., Guo, R., Ke, P., Sun, T., Lu, C., He, P., Wang, Y., Yue, X., Wang, Y., Lei,
1162 Y., Zhou, H., Cai, Z., Wu, Y., Guo, R., Han, T., Xue, J., Boucher, O., Boucher, E.,
1163 Chevallier, F., Tanaka, K., Wei, Y., Zhong, H., Kang, C., Zhang, N., Chen, B., Xi,
1164 F., Liu, M., Bréon, F.-M., Lu, Y., Zhang, Q., Guan, D., Gong, P., Kammen, D. M.,
1165 He, K., and Schellnhuber, H. J.: Near-real-time monitoring of global CO₂

1166 emissions reveals the effects of the COVID-19 pandemic, *Nat. Commun.*, 11,
1167 5172, <https://doi.org/10.1038/s41467-020-18922-7>, 2020b.

1168 Lv, Z., Wang, X., Deng, F., Ying, Q., Archibald, A. T., Jones, R. L., Ding, Y., Cheng,
1169 Y., Fu, M., Liu, Y., Man, H., Xue, Z., He, K., Hao, J., and Liu, H.:
1170 Source–Receptor Relationship Revealed by the Halted Traffic and Aggravated
1171 Haze in Beijing during the COVID-19 Lockdown, *Environ. Sci. Technol.*, 54,
1172 15660-15670, <https://doi.org/10.1021/acs.est.0c04941>, 2020.

1173 Ma, Q., Wang, J., Xiong, M., and Zhu, L.: Air Quality Index (AQI) Did Not Improve
1174 during the COVID-19 Lockdown in Shanghai, China, in 2022, Based on Ground
1175 and TROPOMI Observations, *Remote Sens.*, 15, 1295,
1176 <https://doi.org/10.3390/rs15051295>, 2023.

1177 Ministry of ecology and environment (MEE): The list of technical specifications for
1178 the application and issuance of pollutant discharge permits issued by the ministry
1179 of ecology and environment, 2021.

1180 Ministry of ecology and environment (MEE): Report on the State of the Ecology and
1181 Environment in China, 2022.

1182 MEIC: Multi-resolution Emission Inventory model for Climate and air pollution
1183 research, <http://meicmodel.org.cn/> (last visited on October 2025), 2024.

1184 National Bureau of Statistics of China (NBS): Statistical Yearbook of China, China
1185 Statistics Press, Beijing, 2023 (in Chinese).

1186 Requia, W. J., Di, Q., Silvern, R., Kelly, J. T., Koutrakis, P., Mickley, L. J., Sulprizio,
1187 M. P., Amini, H., Shi, L., and Schwartz, J.: An Ensemble Learning Approach for
1188 Estimating High Spatiotemporal Resolution of Ground-Level Ozone in the
1189 Contiguous United States, *Environ. Sci. Technol.*, 54, 11037-11047,
1190 <https://doi.org/10.1021/acs.est.0c01791>, 2020.

1191 State Council of the People’s Republic of China. Three-year Action Plan for
1192 Protecting Blue Sky. Central Government of the People’s Republic of China
1193 (2018). http://www.gov.cn/zhengce/content/2018-07/03/content_5303158.htm.

1194 Schneider, R., Masselot, P., Vicedo-Cabrera, A. M., Sera, F., Blangiardo, M., Forlani,
1195 C., Douros, J., Jorba, O., Adani, M., Kouznetsov, R., Couvidat, F., Arteta, J.,

1196 Raux, B., Guevara, M., Colette, A., Barré, J., Peuch, V.-H., and Gasparrini, A.:
1197 Differential impact of government lockdown policies on reducing air pollution
1198 levels and related mortality in Europe, *Sci. Rep.*, 12, 726,
1199 <https://doi.org/10.1038/s41598-021-04277-6>, 2022.

1200 Shao, Y., Liu, R., Yang, J., Liu, M., Fang, W., Hu, L., Bi, J., and Ma, Z.: Economic
1201 Growth Facilitates Household Fuel Use Transition to Reduce PM_{2.5}-Related
1202 Deaths in China, *Environ. Sci. Technol.*, 57, 12663-12673,
1203 <https://doi.org/10.1021/acs.est.3c03276>, 2023.

1204 Shen, X., Kong, L., Shi, Y., Cao, X., Li, X., Wu, B., Zhang, H., and Yao, Z.:
1205 Multi-type Air Pollutant Emission Inventory of Non-road Mobile Sources in
1206 China for the Period 1990-2017, *Aerosol Air Qual. Res.*, 21, 210003,
1207 <https://doi.org/10.4209/aaqr.210003>, 2021.

1208 Shen, X., Che, H., Lv, T., Wu, B., Cao, X., Li, X., Zhang, H., Hao, X., Zhou, Q., and
1209 Yao, Z.: Real-world emission characteristics of
1210 semivolatile/intermediate-volatility organic compounds originating from nonroad
1211 construction machinery in the working process, *Sci. Total Environ.*, 858, 159970,
1212 <https://doi.org/10.1016/j.scitotenv.2022.159970>, 2023.

1213 Simayi, M., Shi, Y., Xi, Z., Ren, J., and Xie, S.: Emission trends of industrial VOCs in
1214 China since the clean air action and future reduction perspectives, *Sci. Total
1215 Environ.*, 826, 153994, <https://doi.org/10.1016/j.scitotenv.2022.153994>, 2022.

1216 Sokhi, R. S., Moussiopoulos, N., Baklanov, A., Bartzis, J., Coll, I., Finardi, S.,
1217 Friedrich, R., Geels, C., Grönholm, T., Halenka, T., Ketznel, M., Maragkidou, A.,
1218 Matthias, V., Moldanova, J., Ntziachristos, L., Schäfer, K., Suppan, P., Tsegas, G.,
1219 Carmichael, G., Franco, V., Hanna, S., Jalkanen, J.-P., Velders, G. J. M., and
1220 Kukkonen, J.: Advances in air quality research – current and emerging
1221 challenges, *Atmos. Chem. Phys.*, 22, 4615–4703,
1222 <https://doi.org/10.5194/acp-22-4615-2022>, 2022.

1223 Sun, S., Jin, J., Xia, M., Liu, Y., Gao, M., Zou, C., Wang, T., Lin, Y., Wu, L., Mao, H.,
1224 and Wang, P.: Vehicle emissions in a middle-sized city of China: Current status
1225 and future trends, *Environ. Int.*, 137, 105514,

1226 <https://doi.org/10.1016/j.envint.2020.105514>, 2020.

1227 State Council of the People's Republic of China. Three-year Action Plan for
1228 Protecting Blue Sky. Central People's Government of the People's Republic of
1229 China (2018).
1230 http://www.gov.cn/zhengce/content/2018-07/03/content_5303158.htm.

1231 Tang, L., Qu, J., Mi, Z., Bo, X., Chang, X., Anadon, L. D., Wang, S., Xue, X., Li, S.,
1232 Wang, X., and Zhao, X.: Substantial emission reductions from Chinese power
1233 plants after the introduction of ultra-low emissions standards, *Nat. Energy*, 4,
1234 929-938, <https://doi.org/10.1038/s41560-019-0468-1>, 2019.

1235 Tang, L., Ruan, J., Bo, X., Mi, Z., Wang, S., Dong, G., and Davis, S. J.: Plant-level
1236 real-time monitoring data reveal substantial abatement potential of air pollution
1237 and CO₂ in China's cement sector, *One Earth*, 5, 892-906,
1238 <https://doi.org/10.1016/j.oneear.2022.07.003>, 2022.

1239 Tong, D., Geng, G., Zhang, Q., Cheng, J., Qin, X., Hong, C., He, K., and Davis, S. J.:
1240 Health co-benefits of climate change mitigation depend on strategic power plant
1241 retirements and pollution controls, *Nat. Clim. Chang.*, 11, 1077-1083,
1242 <https://doi.org/10.1038/s41558-021-01216-1>, 2021.

1243 Wang, F., Li, Z., Zhang, K., Di, B., and Hu, B.: An overview of non-road equipment
1244 emissions in China, *Atmos. Environ.*, 132, 283-289,
1245 <https://doi.org/10.1016/j.atmosenv.2016.02.046>, 2016.

1246 Wang, H., He, Q., Kong, H., Qin, K., Zheng, B., Lin, J., and Zhao, Y.: Declining
1247 short-term emission control opportunity for major events in Chinese cities,
1248 *Nature Cities*, 2, 434–446, <https://doi.org/10.1038/s44284-025-00233-x>, 2025.

1249 Wang, K., Gao, J., Tian, H., Dan, M., Yue, T., Xue, Y., Zou, P., and Wang, C.: An
1250 emission inventory spatial allocate method based on POI data, *China Environ.*
1251 *Sci*, 37, 2377-2382, <https://doi.org/10.13198/j.issn.1001-6929.2019.02.13>, 2017.
1252 (in Chinese).

1253 Wang, N., Xu, J., Pei, C., Tang, R., Zhou, D., Chen, Y., Li, M., Deng, X., Deng, T.,
1254 Huang, X., and Ding, A.: Air quality during COVID-19 lockdown in the Yangtze
1255 River Delta and the Pearl River Delta: Two different responsive mechanisms to

1256 emission reductions in China, *Environ. Sci. Technol.*, 55, 5721-5730,
1257 <https://doi.org/10.1021/acs.est.0c08383>, 2021.

1258 Wang, S. W., Zhang, Q., Streets, D. G., He, K. B., Martin, R. V., Lamsal, L. N., Chen,
1259 D., Lei, Y., and Lu, Z.: Growth in NO_x emissions from power plants in China:
1260 bottom-up estimates and satellite observations, *Atmos. Chem. Phys.*, 12,
1261 4429–4447, <https://doi.org/10.5194/acp-12-4429-2012>, 2012.

1262 Wang, L., Liu, D., Yan, W., Kang, Z., Liu, R., Zhang, J., and Li, Z.: Spatio-temporal
1263 distribution, transport characteristics and synoptic patterns of ozone pollution
1264 near surface in Jiangsu province, China, *Atmos. Pollut. Res.*, 13, 101616,
1265 <https://doi.org/10.1016/j.apr.2022.101616>, 2022.

1266 Wang, Y., Zhao, Y., Liu, Y., Jiang, Y., Zheng, B., Xing, J., Liu, Y., Wang, S., and
1267 Nielsen, C. P.: Sustained emission reductions have restrained the ozone pollution
1268 over China, *Nat. Geosci.*, 16, 967-974,
1269 <https://doi.org/10.1038/s41561-023-01284-2>, 2023.

1270 Wei, X., Tong, Q., Magill, I., Vithaya, P., and Betz, R.: Evaluation of potential
1271 co-benefits of air pollution control and climate mitigation policies for China's
1272 electricity sector, <https://doi.org/10.1016/j.eneco.2020.104917>, 2020.

1273 Xiao, Q., Chang, H., Geng, G., and Liu, Y.: An Ensemble Machine-Learning Model
1274 To Predict Historical PM_{2.5} Concentrations in China from Satellite Data, *Environ.*
1275 *Sci. Technol.*, 52, 13260-13269, <https://doi.org/10.1021/acs.est.8b02917>, 2018.

1276 Xu, Y., Chen, S., Wang, Z., Liu, B., and Wang, L.: Multi-Scale Dynamics and Spatial
1277 Consistency of Economy and Population Based on NPP/VIIRS Nighttime Light
1278 Data and Population Imagery: A Case Study of the Yangtze River Delta, *Remote*
1279 *Sens.*, 16, 2806, <https://doi.org/10.3390/rs16152806>, 2024.

1280 Xu, R., Tong, D., Xiao, Q., Qin, X., Chen, C., Yan, L., Cheng, J., Cui, C., Hu, H., Liu,
1281 W., Yan, X., Wang, H., Liu, X., Geng, G., Lei, Y., Guan, D., He, K., and Zhang,
1282 Q. MEIC-global-CO₂: A new global CO₂ emission inventory with
1283 highly-resolved source category and sub-country information, *Sci. China Earth*
1284 *Sci.*, 66, doi: <https://doi.org/10.1007/s11430-023-1230-3>, 2023.

1285 Yang, X. F., Liu, H., Man, H. Y., and He, K. B.: Characterization of road freight

1286 transportation and its impact on the national emission inventory in China, *Atmos.*
1287 *Chem. Phys.*, 15, 2105–2118, <https://doi.org/10.5194/acp-15-2105-2015>, 2015.

1288 Yang, D., Zhang, S., Niu, T., Wang, Y., Xu, H., Zhang, K. M., and Wu, Y.:
1289 High-resolution mapping of vehicle emissions of atmospheric pollutants based
1290 on large-scale, real-world traffic datasets, *Atmos. Chem. Phys.*, 19, 8831–8843,
1291 <https://doi.org/10.5194/acp-19-8831-2019>, 2019.

1292 Yang, L., Hu, Y.-J., Wang, H., Li, C., Tang, B.-J., Wang, B., and Cui, H.: Uncertainty
1293 quantification of CO₂ emissions from China's civil aviation industry to 2050, *J.*
1294 *Environ. Manage.*, 336, 117624, <https://doi.org/10.1016/j.jenvman.2023.117624>,
1295 2023.

1296 Yun, X., Meng, W., Xu, H., Zhang, W., Yu, X., Shen, H., Chen, Y., Shen, G., Ma, J., Li,
1297 B., Cheng, H., Hu, J., and Tao, S.: Coal Is Dirty, but Where It Is Burned
1298 Especially Matters, *Environ. Sci. Technol.*, 55, 7316–7326,
1299 <https://doi.org/10.1021/acs.est.1c01148>, 2021.

1300 Zhan, Y., Xie, M., Zhao, W., Wang, T., Gao, D., Chen, P., Tian, J., Zhu, K., Li, S.,
1301 Zhuang, B., Li, M., Luo, Y., and Zhao, R.: Quantifying the seasonal variations in
1302 and regional transport of PM_{2.5} in the Yangtze River Delta region, China:
1303 characteristics, sources, and health risks, *Atmos. Chem. Phys.*, 23, 9837–9852,
1304 <https://doi.org/10.5194/acp-23-9837-2023>, 2023.

1305 Zhang, B., Zhang, J., and Feng, T.: A global comparative study on the impact of
1306 COVID-19 policy on atmospheric nitrogen dioxide (NO₂): Evidence from remote
1307 sensing data in 2019–2022, *J. Environ. Manage.*, 367, 121851,
1308 <https://doi.org/10.1016/j.jenvman.2024.121851>, 2024.

1309 Zhang, Q., Zheng, Y., Tong, D., Shao, M., Wang, S., Zhang, Y., Xu, X., Wang, J., He,
1310 H., Liu, W., Ding, Y., Lei, Y., Li, J., Wang, Z., Zhang, X., Wang, Y., Cheng, J.,
1311 Liu, Y., Shi, Q., Yan, L., Geng, G., Hong, C., Li, M., Liu, F., Zheng, B., Cao, J.,
1312 Ding, A., Gao, J., Fu, Q., Huo, J., Liu, B., Liu, Z., Yang, F., He, K., and Hao, J.:
1313 Drivers of improved PM_{2.5} air quality in China from 2013 to 2017, *Proc. Natl.*
1314 *Acad. Sci.*, 116, 24463–24469, <https://doi.org/10.1073/pnas.1907956116>, 2019.

1315 Zhang, S., Zhang, C., Cai, W., Bai, Y., Callaghan, M., Chang, N., Chen, B., Chen, H.,

1316 Cheng, L., Dai, H., Dai, X., Fan, W., Fang, X., Gao, T., Geng, Y., Guan, D., Hu,
1317 Y., Hua, J., Huang, C., Huang, H., Huang, J., Huang, X., Ji, J. S., Jiang, Q., Jiang,
1318 X., Kieser, G., Li, T., Liang, L., Lin, B., Lin, H., Liu, H., Liu, Q., Liu, X., Liu, Z.,
1319 Liu, Z., Liu, Y., Lu, B., Lu, C., Luo, Z., Ma, W., Mi, Z., Ren, C., Romanello, M.,
1320 Shen, J., Su, J., Sun, Y., Sun, X., Tang, X., Walawender, M., Wang, C., Wang, Q.,
1321 Wang, R., Warnecke, L., Wei, W., Wen, S., Xie, Y., Xiong, H., Xu, B., Yan, Y.,
1322 Yang, X., Yao, F., Yu, L., Yuan, J., Zeng, Y., Zhang, J., Zhang, L., Zhang, R.,
1323 Zhang, S., Zhang, S., Zhao, M., Zheng, D., Zhou, H., Zhou, J., Zhou, Z., Luo, Y.,
1324 and Gong, P.: The 2023 China report of the Lancet Countdown on health and
1325 climate change: taking stock for a thriving future, *The Lancet Public Health*, 8,
1326 e978-e995, [https://doi.org/10.1016/S2468-2667\(23\)00245-1](https://doi.org/10.1016/S2468-2667(23)00245-1), 2023.

1327 Zhang, Y., Yang, X., Brown, R., Yang, L., Morawska, L., Ristovski, Z., Fu, Q., and
1328 Huang, C.: Shipping emissions and their impacts on air quality in China, *Sci.*
1329 *Total Environ.*, 581, 186-198, <https://doi.org/10.1016/j.scitotenv.2016.12.098>,
1330 2017.

1331 Zhang, Y., Bo, X., Zhao, Y., and Nielsen, C. P.: Benefits of current and future policies
1332 on emissions of China's coal-fired power sector indicated by continuous emission
1333 monitoring, *Environ. Pollut.*, 251, 415-424,
1334 <https://doi.org/10.1016/j.envpol.2019.05.021>, 2019.

1335 Zhao, Y., Wang, S., Nielsen, C. P., Li, X., and Hao, J.: Establishment of a database of
1336 emission factors for atmospheric pollutants from Chinese coal-fired power plants,
1337 *Atmos. Environ.*, 44, 1515-1523, <https://doi.org/10.1016/j.atmosenv.2010.01.017>,
1338 2010.

1339 Zhao, Y., Zhang, J., and Nielsen, C. P.: The effects of recent control policies on trends
1340 in emissions of anthropogenic atmospheric pollutants and CO₂ in China, *Atmos.*
1341 *Chem. Phys.*, 13, 487-508, <https://doi.org/10.5194/acp-13-487-2013>, 2013.

1342 Zhao, Y., Zhang, K., Xu, X., Shen, H., Zhu, X., Zhang, Y., Hu, Y., and Shen, G.:
1343 Substantial Changes in Nitrogen Dioxide and Ozone after Excluding
1344 Meteorological Impacts during the COVID-19 Outbreak in Mainland China,
1345 *Environ. Sci. Technol. Let.*, 7, 402-408,

1346 <https://doi.org/10.1021/acs.estlett.0c00304>, 2020a.

1347 Zhao, Y., Yuan, M., Huang, X., Chen, F., and Zhang, J.: Quantification and evaluation
1348 of atmospheric ammonia emissions with different methods: a case study for the
1349 Yangtze River Delta region, China, *Atmos. Chem. Phys.*, 20, 4275–4294,
1350 <https://doi.org/10.5194/acp-20-4275-2020>, 2020b.

1351 Zhao, S., Hu, B., Liu, H., Du, C., Xia, X., and Wang, Y.: The influence of aerosols on
1352 the NO₂ photolysis rate in a suburban site in North China, *Sci. Total Environ.*,
1353 144788, <https://doi.org/10.1016/j.scitotenv.2020.144788>, 2021.

1354 Zhao, Y., Xi, M., Zhang, Q., Dong, Z., Ma, M., Zhou, K., Xu, W., Xing, J., Zheng, B.,
1355 Wen, Z., Liu, X., Nielsen, C. P., Liu, Y., Pan, Y., and Zhang, L.: Decline in bulk
1356 deposition of air pollutants in China lags behind reductions in emissions, *Nat.*
1357 *Geosci.*, 15, 190–195, <https://doi.org/10.1038/s41561-022-00899-1>, 2022.

1358 Zhao, X., Shao, B., Su, J., and Tian, N.: Exploring synergistic evolution of carbon
1359 emissions and air pollutants and spatiotemporal heterogeneity of influencing
1360 factors in Chinese cities, *Sci. Rep.*, 15, 2657,
1361 <https://doi.org/10.1038/s41598-024-84212-7>, 2025.

1362 Zheng, B., Tong, D., Li, M., Liu, F., Hong, C., Geng, G., Li, H., Li, X., Peng, L., Qi, J.,
1363 Yan, L., Zhang, Y., Zhao, H., Zheng, Y., He, K., and Zhang, Q.: Trends in China's
1364 anthropogenic emissions since 2010 as the consequence of clean air actions,
1365 *Atmos. Chem. Phys.*, 18, 14095–14111,
1366 <https://doi.org/10.5194/acp-18-14095-2018>, 2018.

1367 Zheng, B., G. Geng, P. Ciais, S. J. Davis, R. V. Martin, J. Meng, N. Wu, F. Chevallier,
1368 G. Broquet, F. Boersma, R. J. van der A, J. Lin, D. Guan, Y. Lei, K. He, Q.
1369 Zhang. Satellite-based estimates of decline and rebound in China's CO₂
1370 emissions during COVID-19 pandemic. *Sci. Adv.*, 6, eabd4998,
1371 <https://doi.org/10.1126/sciadv.abd4998>, 2020.

1372 Zheng, B., Zhang, Q., Geng, G., Chen, C., Shi, Q., Cui, M., Lei, Y., and He, K.:
1373 Changes in China's anthropogenic emissions and air quality during the
1374 COVID-19 pandemic in 2020, *Earth Syst. Sci. Data*, 13, 2895–2907,
1375 <https://doi.org/10.5194/essd-13-2895-2021>, 2021.

1376 Zhou, Y., Zhao, Y., Mao, P., Zhang, Q., Zhang, J., Qiu, L., and Yang, Y.: Development
1377 of a high-resolution emission inventory and its evaluation and application
1378 through air quality modeling for Jiangsu Province, China, *Atmos. Chem. Phys.*,
1379 17, 211–233, <https://doi.org/10.5194/acp-17-211-2017>, 2017.

1380 Zhou, Z., Tan, Q., Liu, H., Deng, Y., Wu, K., Lu, C., and Zhou, X.: Emission
1381 characteristics and high-resolution spatial and temporal distribution of pollutants
1382 from motor vehicles in Chengdu, China, *Atmos. Pollut. Res.*, 10, 749-758,
1383 <https://doi.org/10.1016/j.apr.2018.12.002>, 2019.

1384 Zhou, K., Xu, W., Zhang, L., Ma, M., Liu, X., and Zhao, Y.: Estimating nitrogen and
1385 sulfur deposition across China during 2005 to 2020 based on multiple statistical
1386 models, *Atmos. Chem. Phys.*, 23, 8531–8551,
1387 <https://doi.org/10.5194/acp-23-8531-2023>, 2023.

1388

1389 **Figure captions**

1390 **Figure 1** The research framework of near-real-time emission estimation and
1391 application in this work.

1392 **Figure 2** Daily emission estimates of anthropogenic air pollutants by sector for
1393 Jiangsu Province in 2022. (a) NO_x; (b) SO₂; (c) PM_{2.5}; (d) NMVOCs; (e) NH₃.

1394 **Figure 3** Spatial distribution of anthropogenic NO_x emissions for Jiangsu Province in
1395 2022 with a horizontal resolution of 3 × 3 km. (a) Total emissions; (b) Power; (c)
1396 Industry; (d) Vehicle; (e) Off-road transportation; (f) Residential. The map data
1397 provided by Resource and Environment Data Cloud Platform are freely available for
1398 academic use (<http://www.resdc.cn/data.aspx?DATAID=201>), © Institute of
1399 Geographic Sciences & Natural Resources Research, Chinese Academy of Sciences.

1400 **Figure 4** The monthly air pollutant emissions for Jiangsu Province in 2022 estimated
1401 in this study (a, c, and e) and in national emission inventory (MEIC; b, d, and f). The
1402 emissions of SO₂ (a and b), NO_x (c and d) and primary PM_{2.5} (e and f) are contained.
1403 The red lines with triangles represent the observed monthly surface concentrations of

1404 corresponding air pollutants.

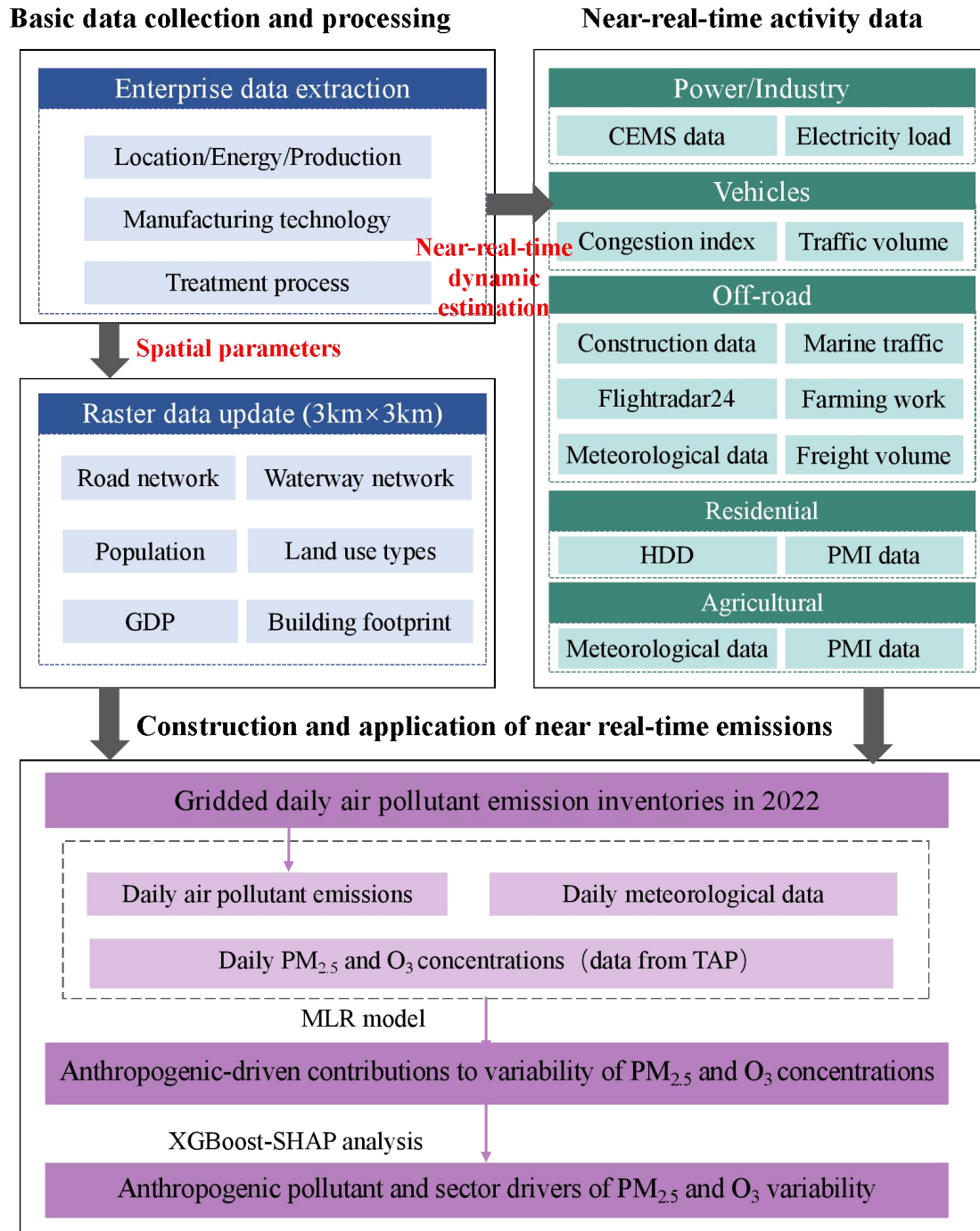
1405 **Figure 5** The differences between the emissions of NO_x (a), SO₂ (b), PM_{2.5} (c) and
1406 NMVOCs (d) in April-May for 2022 and 2023 in Jiangsu Province. The first column
1407 illustrates the daily total emissions and the differences for the period of the two years.
1408 The second column illustrates the contributions of various source categories to the
1409 differences in daily total emissions, and the third column aggregates them for the
1410 whole period.

1411 **Figure 6** Comparison between the observed daily PM_{2.5} concentrations (blue lines)
1412 and the simulated concentrations with different emission inventories in Jiangsu
1413 Province for January (a), April (b), July (c), and October (d) in 2022. The simulations
1414 were conducted using the near-real-time emission inventory developed in this work
1415 (red lines) and the revised national emission inventory MEIC (MEIC-revision, black
1416 lines). See Section 2.3 for the rationale of MEIC revision.

1417 **Figure 7** Comparison between the observed daily maximum 8-hour average (MDA8)
1418 O₃ concentrations and the simulated concentrations with different emission
1419 inventories in Jiangsu Province for January (a), April (b), July (c), and October (d) in
1420 2022. The simulations were conducted using the near-real-time emission inventory
1421 developed in this work (red lines) and the revised national emission inventory MEIC
1422 (MEIC-revision, black lines). See Section 2.3 for the rationale of MEIC revision.

1423 **Figure 8** The monthly anomaly in PM_{2.5} (a) and MDA8 O₃ concentrations (b) driven
1424 by the changing daily emissions for Jiangsu Province in 2022, based on the MLR
1425 model.

1426 **Figure 9** Anthropogenic pollutant and sector drivers of PM_{2.5} and MDA8 O₃
1427 variability. (a) and (b) illustrate the contributions of pollutant-sector combinations to
1428 the variability of PM_{2.5} in January and that of O₃ in July, derived from SHAP analysis.
1429 The black dashed lines represent the observed daily ground-level concentrations of
1430 PM_{2.5} and MDA8 O₃. (c) and (d) provided the contributions of the changing emissions
1431 from different sectors, with those of various precursor species aggregated.



1432

1433 **Figure 1** The research framework of near-real-time emission estimation and
 1434 application in this work.

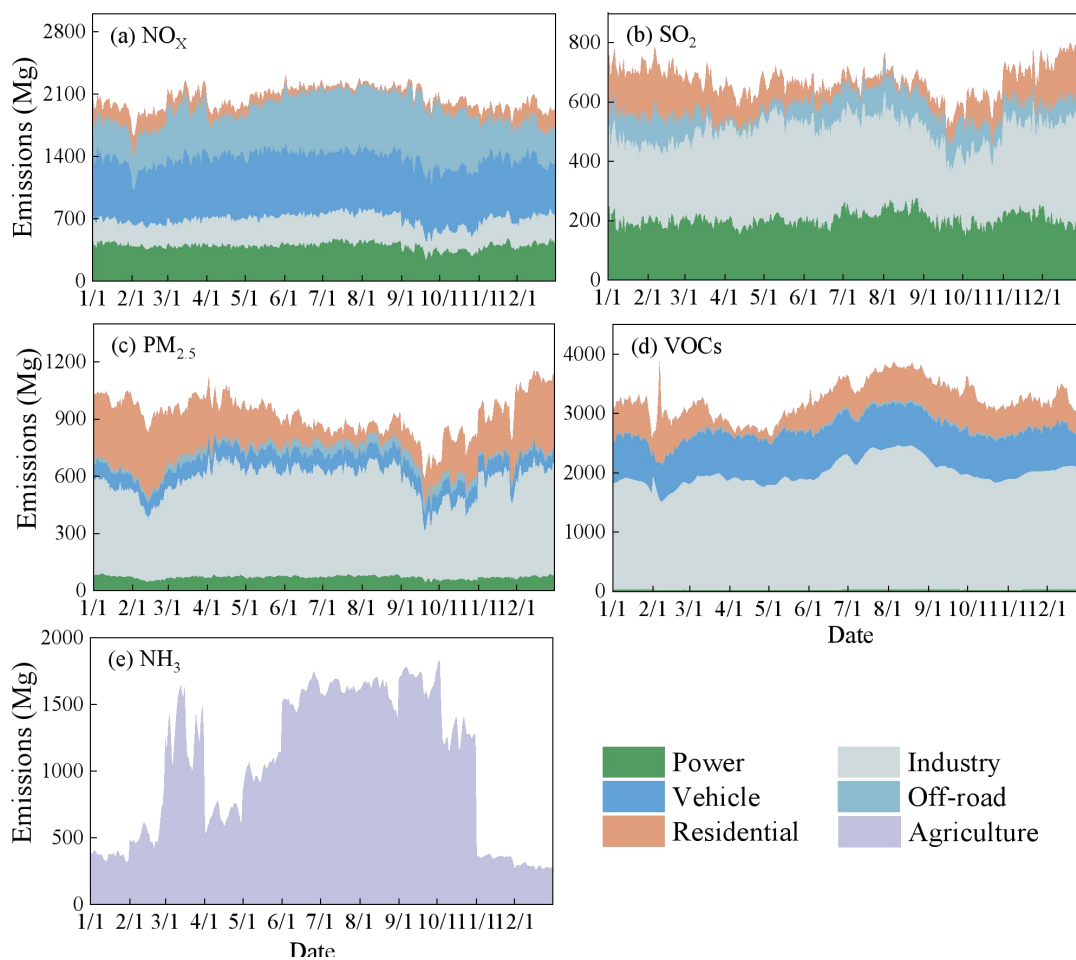


Figure 2 Daily emission estimates of anthropogenic air pollutants by sector for Jiangsu Province in 2022. (a) NO_x ; (b) SO_2 ; (c) $\text{PM}_{2.5}$; (d) NMVOCs; (e) NH_3 .

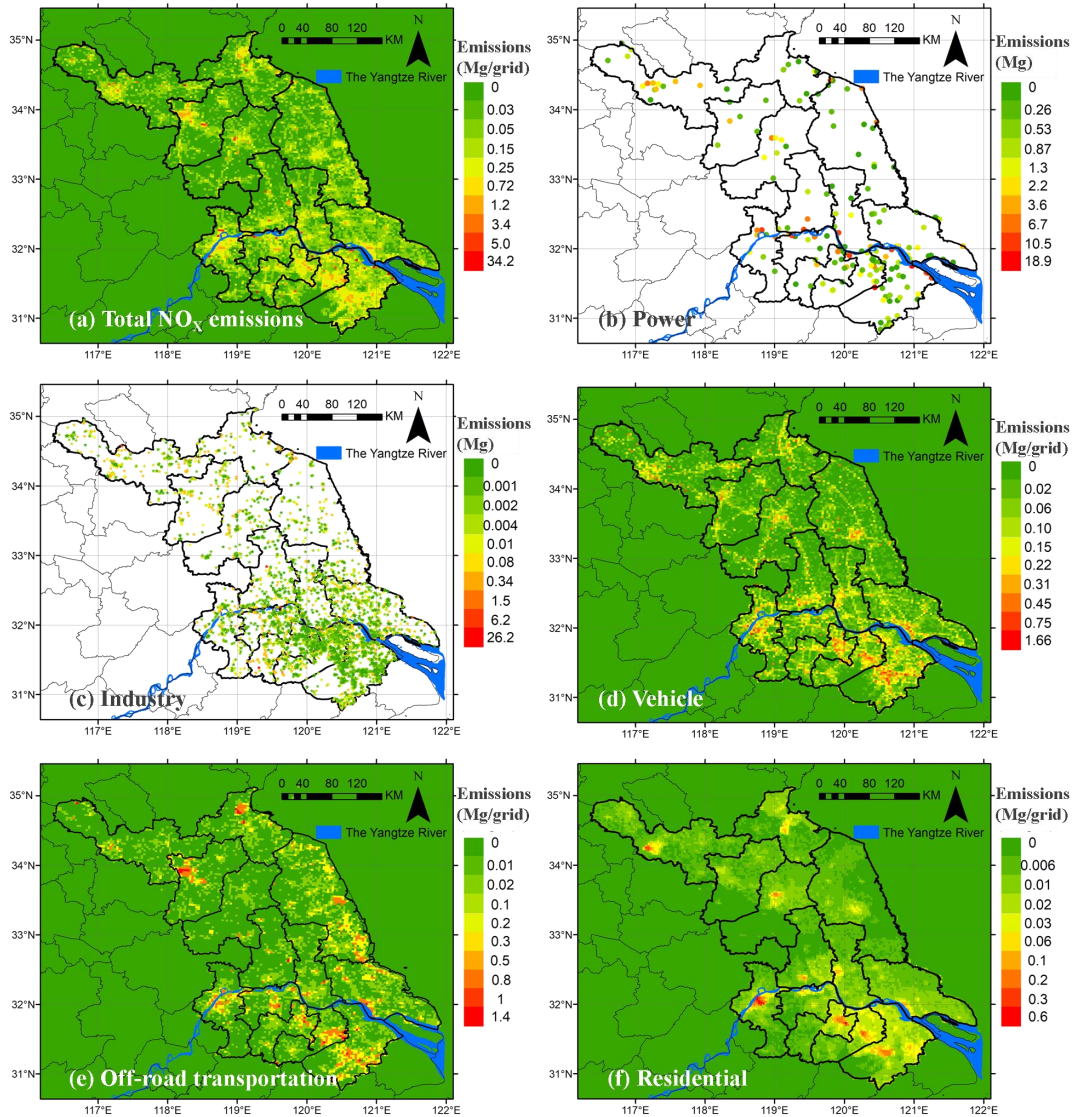


Figure 3 Spatial distribution of anthropogenic NO_x emissions for Jiangsu Province in 2022 with a horizontal resolution of 3×3 km. (a) Total emissions; (b) Power; (c) Industry; (d) Vehicle; (e) Off-road transportation; (f) Residential. The map data provided by Resource and Environment Data Cloud Platform are freely available for academic use (<http://www.resdc.cn/data.aspx?DATAID=201>), © Institute of Geographic Sciences & Natural Resources Research, Chinese Academy of Sciences.

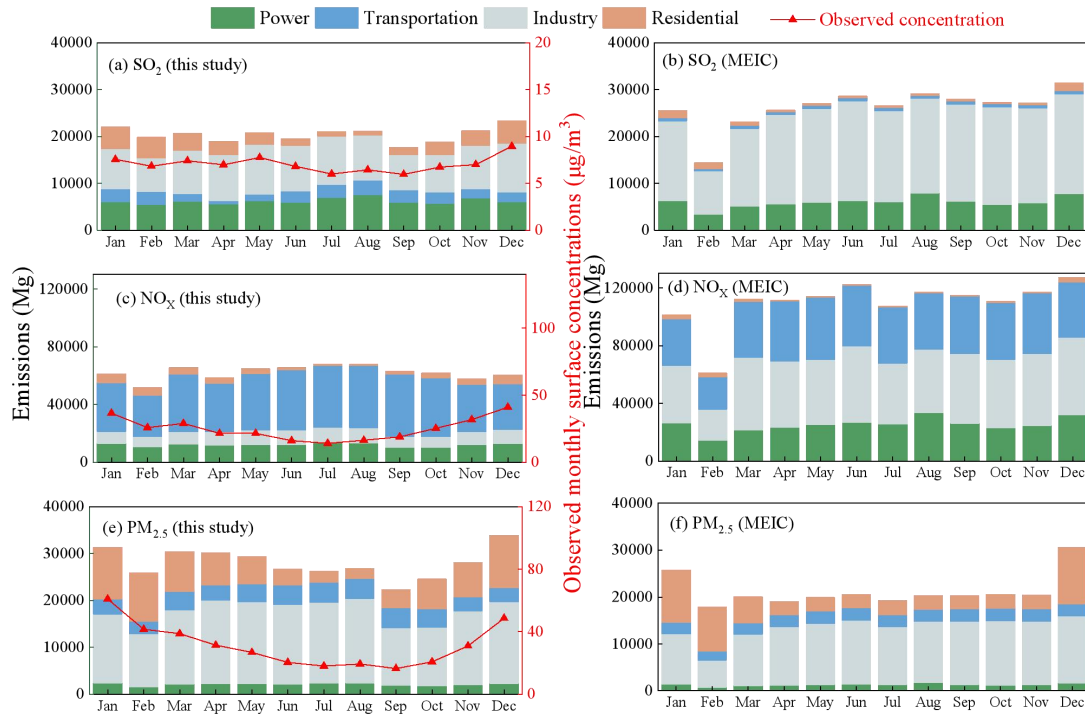


Figure 4 The monthly air pollutant emissions for Jiangsu Province in 2022 estimated in this study (a, c, and e) and in national emission inventory (MEIC; b, d, and f). The emissions of SO₂ (a and b), NO_x (c and d) and primary PM_{2.5} (e and f) are contained. The red lines with triangles represent the observed monthly surface concentrations of corresponding air pollutants.

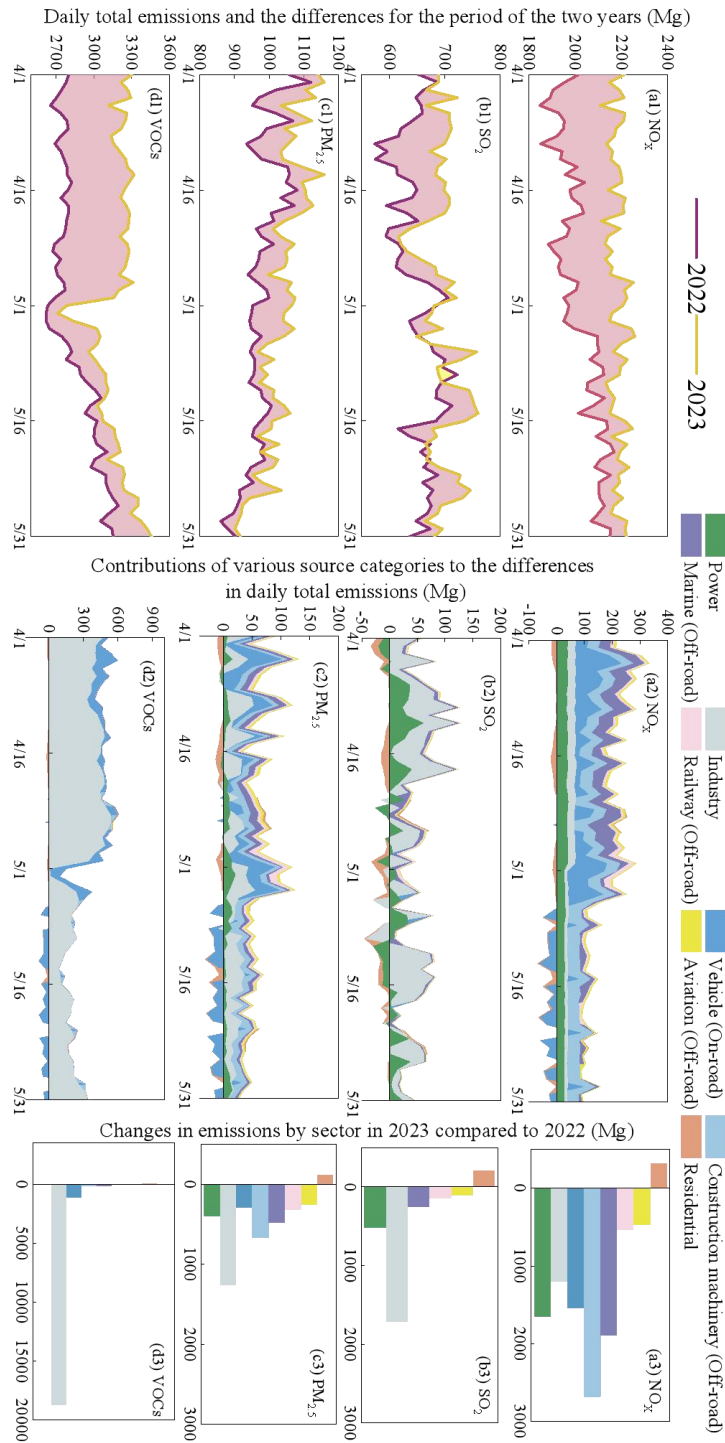


Figure 5 The differences between the emissions of NO_x (a), SO_2 (b), $\text{PM}_{2.5}$ (c) and NMVOCs (d) in April-May for 2022 and 2023 in Jiangsu Province. The first column illustrates the daily total emissions and the differences for the period of the two years. The second column illustrates the contributions of various source categories to the differences in daily total emissions, and the third column aggregates them for the whole period.

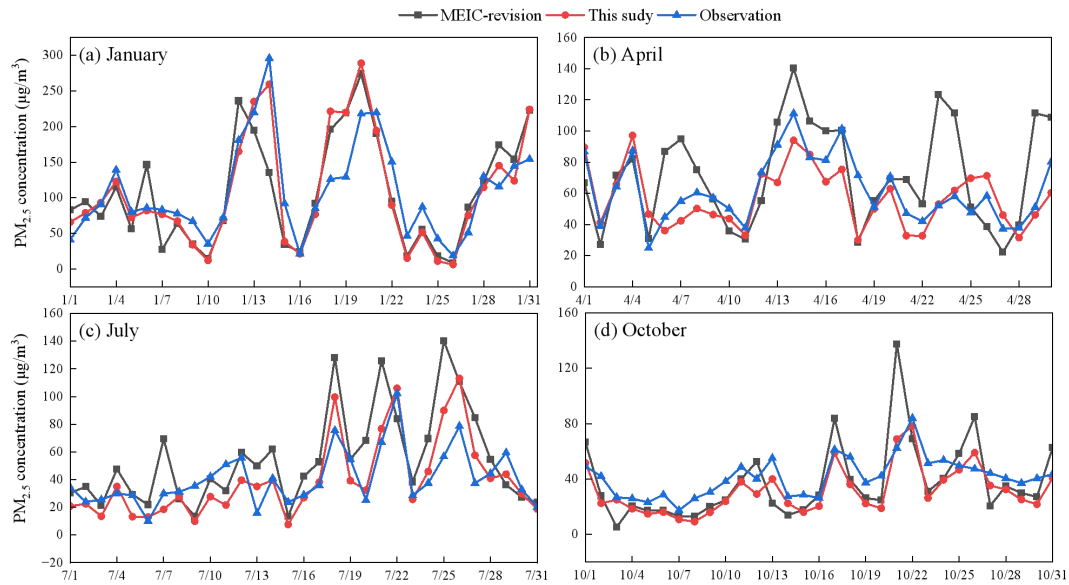


Figure 6 Comparison between the observed daily $PM_{2.5}$ concentrations (blue lines) and the simulated concentrations with different emission inventories in Jiangsu Province for January (a), April (b), July (c), and October (d) in 2022. The simulations were conducted using the near-real-time emission inventory developed in this work (red lines) and the revised national emission inventory MEIC (MEIC-revision, black lines). See Section 2.3 for the rationale of MEIC revision.

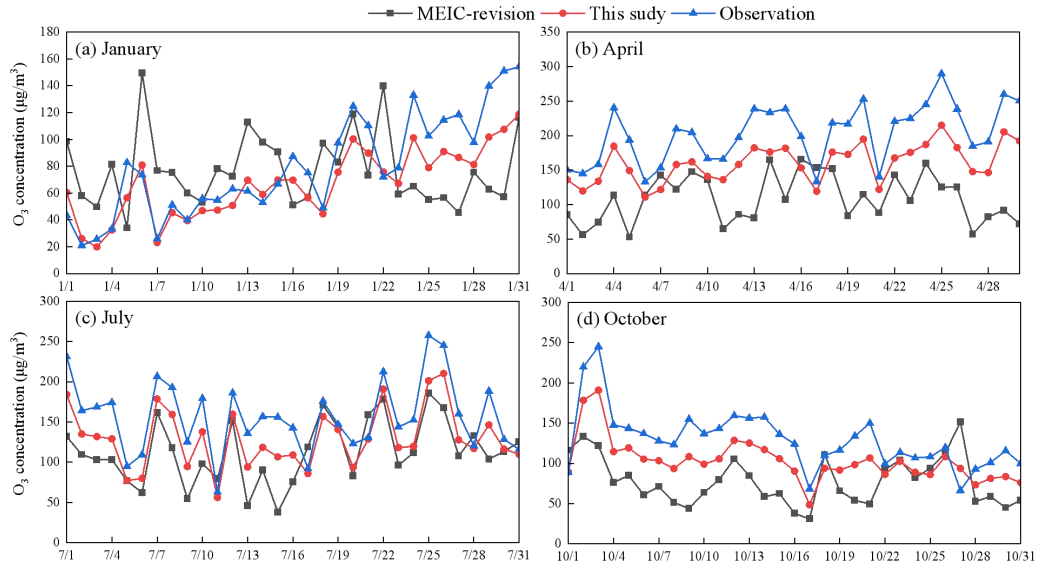


Figure 7 Comparison between the observed daily maximum 8-hour average (MDA8) O_3 concentrations and the simulated concentrations with different emission inventories in Jiangsu Province for January (a), April (b), July (c), and October (d) in 2022. The simulations were conducted using the near-real-time emission inventory developed in this work (red lines) and the revised national emission inventory MEIC (MEIC-revision, black lines). See Section 2.3 for the rationale of MEIC revision.

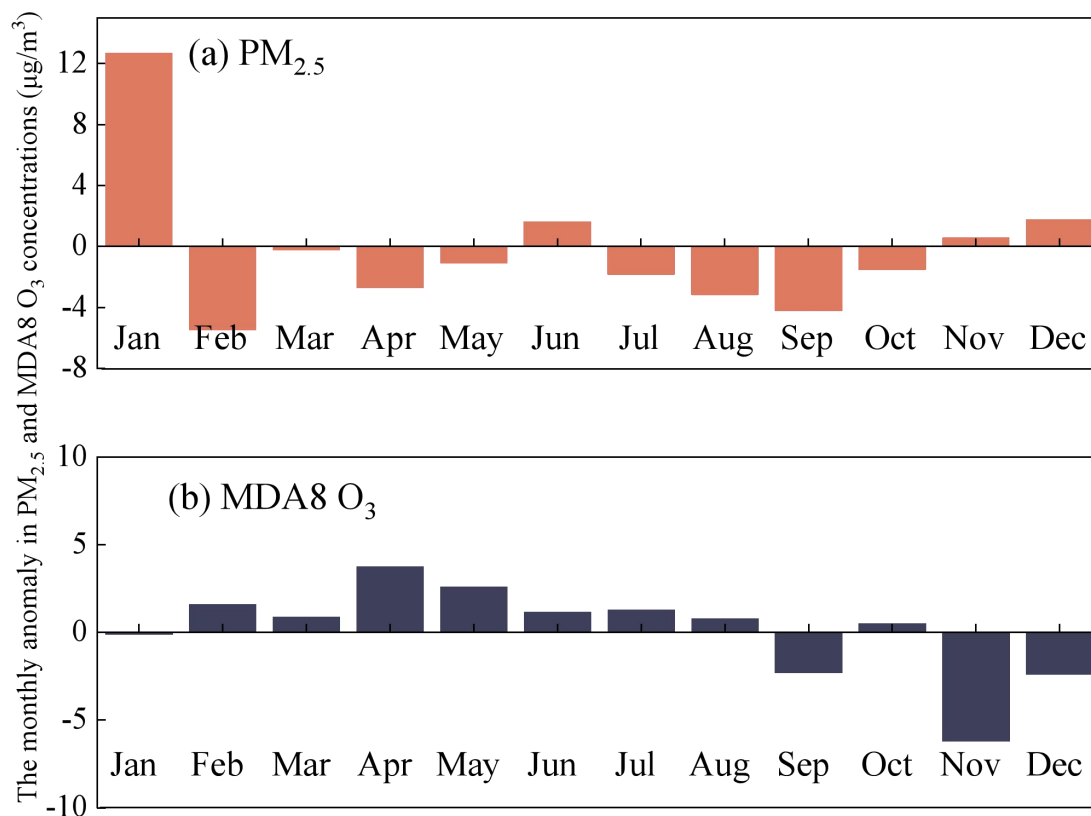


Figure 8 The monthly anomaly in PM_{2.5} (a) and MDA8 O₃ concentrations (b) driven by the changing daily emissions for Jiangsu Province in 2022, based on the MLR model.

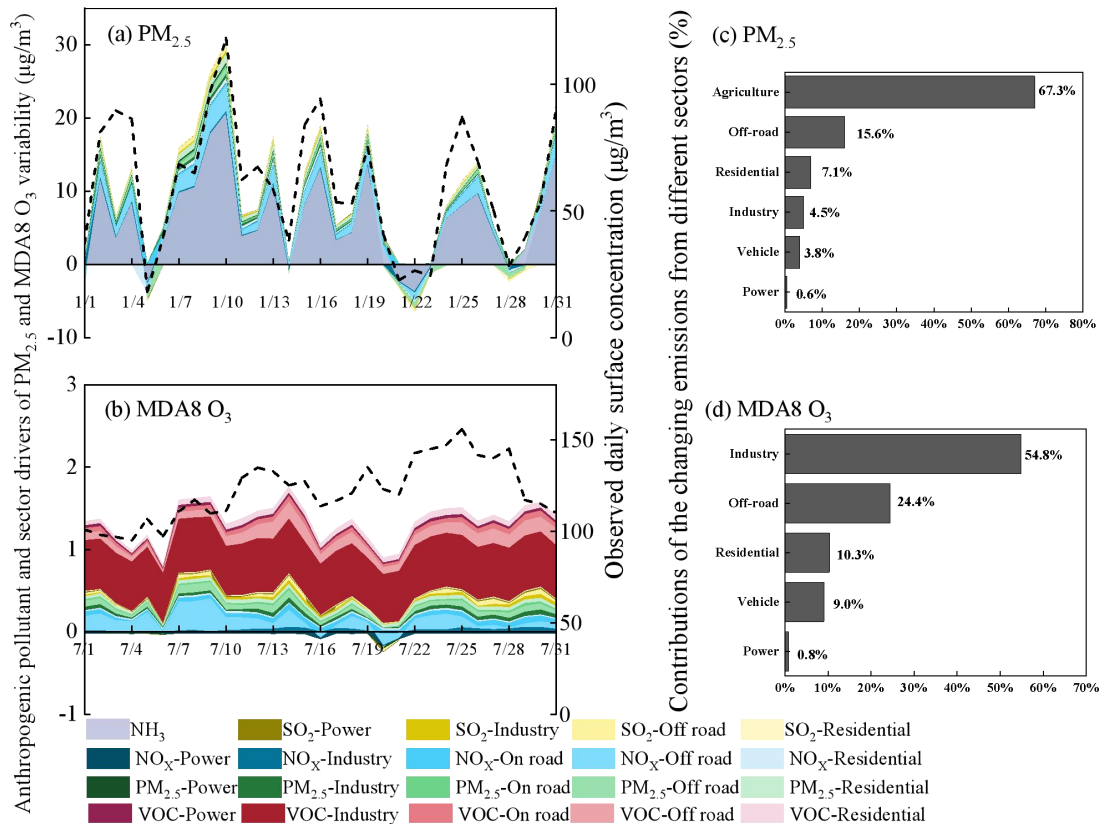


Figure 9 Anthropogenic pollutant and sector drivers of PM_{2.5} and MDA8 O₃ variability. (a) and (b) illustrate the contributions of pollutant-sector combinations to the variability of PM_{2.5} in January and that of O₃ in July, derived from SHAP analysis. The black dashed lines represent the observed daily ground-level concentrations of PM_{2.5} and MDA8 O₃. (c) and (d) provided the contributions of the changing emissions from different sectors, with those of various precursor species aggregated.